Geoderma 404 (2021) 115295

Contents lists available at ScienceDirect

Geoderma

journal homepage: www.elsevier.com/locate/geoderma

Rainfall is the major driver of plant Si availability in perudic gibbsitic Andosols

Charles Vander Linden [a], Zimin Li [a,*], Anne Iserentant [a], Eric Van Ranst [b], Félix de Tombeur [c], Bruno Delvaux [a]

[a] Université catholique de Louvain (UCLouvain), Earth and Life Institute, Soil Science, Croix du Sud 2/L7.05.10, 1348 Louvain-la-Neuve, Belgium
[b] Department of Geology (WE13), Ghent University, Krijgslaan 281, Campus Sterre S8, B-9000 Gent, Belgium
[c] BIOSE Department, Gembloux Agro-Bio Tech, University of Liège, 5030 Gembloux, Belgium

ARTICLE INFO

Handling Editor: David Laird

Keywords:
Perhydrated gibbsitic Andosols
Plant available silicon
Rainfall
Desilication
Phytolith

ABSTRACT

The amount of water available to leach solutes from soil is one of the major features determining mineral weathering, mineral neoformation and soil properties. It affects the fate of dissolved silicon (Si), which may follow four routes: leaching, mineral synthesis, adsorption, uptake by plants forming phytoliths. Here, we quantify the reservoirs of bioavailable Si and phytolithic Si in topsoils (0–20 cm) from wet tropical Andosols along a climosequence where mean annual rainfall (MAR) increases from 2650 to 4400 mm with increasing altitude (65–375 m asl) in Basse-Terre, Guadeloupe. We assessed bioavailable Si through $CaCl_2$ extraction in soil, and foliar analysis in banana plants. We evaluated the pool of phytolithic Si through Na_2CO_3 extraction and heavy liquid separation. The Na_2CO_3 extraction was performed on both the bulk soil and oxalate–treated soil (ox-Na_2CO_3) cleared of its amorphous aluminosilicates. The Andosols have reached an advanced weathering stage. Their secondary products included (Al, Fe)–humus complexes, ferrihydrite, gibbsite, poorly crystalline Al hydroxide, and aluminous allophanic substances. The contents of organic C, metal-humus, ferrihydrite and gibbsite increased in soils in the wettest conditions (>3000 mm) whereas allophane content concomitantly decreased. Silicon leaf content varied little (3.8–5.3 g kg^{-1}), but slightly decreased with increasing MAR ($r = -0.48$). Bioavailable Si content in soil decreased from 63 to 12 mg kg^{-1} with increasing MAR ($r = -0.92$), and was strongly correlated ($r = +0.95$) to that of phytolithic Si as assessed after ox-Na_2CO_3 extraction, linked to fresh, labile phytoliths. The Si/Al atomic ratio of the ox-Na_2CO_3 extract regularly decreased from 1.06 to 0.37 with increasing MAR, hence corroborating strongest desilication in soils in the wettest conditions. In these highly leached, gibbsitic Andosols, rainfall is thus the major driver of plant Si availability.

1. Introduction

In soils experiencing net acidification (van Breemen et al., 1983), weatherable primary silicates inherited from parent materials (lithogenic silicates, LSi) dissolve and release monosilicic acid ($H_4SiO_4^0$), aluminum (Al), iron (Fe) and other aqueous solutes. The solutes may recombine to synthesize pedogenic secondary silicates (PSi), or precipitate as oxides, i.e. Al and Fe (Garrels and Christ, 1965). Through its impact on solute concentration and fate, rainfall, in particular the amount of water available to leach solutes from soil, is one of the major features determining mineral weathering, secondary mineral synthesis and soil properties (Garrels and Christ, 1965; Rai and Kittrick, 1989). For instance, in volcanic soils derived from basalt, the water regime strongly imprints soil processes and mineral composition, and fixes steep thresholds that define soil properties, buffering capacity and their biogeochemical behavior (Chadwick et al., 2003). The fate of silicon (Si) is crucial, given its role in mineral synthesis (Garrels and Christ, 1965). Once released, aqueous $H_4SiO_4^0$ may take four routes: (i) leaching and export to watersheds (Bartoli, 1983); (ii) synthesis of clay minerals (Garrels and Christ, 1965) and/or silica, either amorphous (Drees et al., 1989) or possibly crystalline (Eswaran, 1972; Monger and Kelly, 2002); (iii) adsorption on Fe and Al oxides (Beckwith and Reeve, 1963; Jones and Handreck, 1963; McKeague and Cline, 1963); (iv) uptake by plant roots (Jones and Handreck, 1965; Bartoli, 1983). Abundant precipitation and intense leaching enhance mineral weathering and export of solutes to watersheds. Secondary minerals synthesized from dilute

* Corresponding author.
E-mail address: zimin.li@uclouvain.be (Z. Li).

https://doi.org/10.1016/j.geoderma.2021.115295
Received 24 January 2021; Received in revised form 4 June 2021; Accepted 7 June 2021

solutions include aluminosilicates with low Si/Al ratio, and Al and Fe oxides. In perhumid volcanic ash soils, typical compositions encompass allophane, imogolite, gibbsite and ferrihydrite as well as (Al, Fe)-humus complexes if soil organic matter (SOM) accumulates (Colmet-Daage and Lagache, 1965; Huang et al., 2002; Jongmans et al., 1994; Ndayiragije and Delvaux, 2003; Nieuwenhuyse and van Breemen, 1997; Nizeyimana et al., 1997; Parfitt et al., 1983; Parfitt and Wilson, 1985). Apart through mineral synthesis, aqueous $H_4SiO_4^0$ can also be retrieved from soil solution through adsorption on oxide surfaces and root uptake. Plants absorb $H_4SiO_4^0$ and form amorphous silica bodies ($SiO_2{\cdot}nH_2O$, opal A) called phytoliths (Jones and Handreck, 1965; Piperno, 1988; Raven, 1983; Sangster and Hodson, 1986). Silicon returns to soil through phytolith deposition within plant debris (Smithson, 1956; Lucas et al., 1993). In soil, phytoliths readily dissolve at common pH values of soil solution (Fraysse et al., 2009) and contribute to supply the pool of dissolved Si (DSi) (Bartoli, 1983; Derry et al., 2005; Lucas et al., 1993). The Si uptake by roots, phytolith formation in plant and dissolution in soil providing bioavailable Si for plant uptake defines a biological Si feedback loop, which governs the terrestrial biogeochemical cycle of Si (e.g. Alexandre et al., 1997; Bartoli, 1983; Henriet et al., 2008a; Lucas et al., 1993; Meunier et al., 1999). Because of mineral depletion, this loop may be particularly active in highly weathered, desilicated soils (Cornelis and Delvaux, 2016) depending on land use (Vander Linden and Delvaux, 2019). This biological effect keeps Si from being leached, and accounts for the stability of kaolinite in the surface horizons of gibbsitic ferrallitic soils in humid tropical conditions (Lucas et al., 1993). In arid and semi-arid conditions, increasing water availability increases the Si uptake by plants, as measured in Israel (MAR ranging from 80 to 900 mm) (Katz et al., 2013) as well as in grasslands in the Great Plains (MAR ranging from 340 to 1110 mm) (Blecker et al., 2006). In Serengeti savanna ecosystems under MAR ranging from 600 to 900 mm, Quigley et al. (2017) identified soil pH, sand content and, to a lesser extent, rainfall as drivers controlling dissolved Si and soil phytogenic Si pools. Following Chadwick et al. (2003), at MAR above 1400 mm, soil buffering capacity has been totally exhausted in basalt-derived soils from Hawaii. Yet the biological cycling of Si may alleviate natural soil desilication (Lucas et al., 1993), and "buffer" the release of plant available Si to some extent as demonstrated experimentally (Li et al., 2020a). In humid tropical forests under MAR ranging from 1600 to 3200 mm, Schaller et al. (2018) identified soil weathering stage and pH as drivers of plant available Si, but not rainfall.

The impact of rainfall on Si bioavailability in the humid tropics is thus poorly known. Here, we quantify the reservoirs of bioavailable Si and phytolithic Si in perhumid volcanic ash soils along a climosequence where MAR increases from 2650 to 4400 mm with increasing altitude (65–375 m above sea level (asl)) in the volcanic island of Basse-Terre, Guadeloupe.

2. Environmental framework

The study area is located in the Pères River catchment on the eastern flank of *La Soufrière* volcano, south-east of the Basse-Terre Island in Guadeloupe (16°N, 61°W) (Fig. 1a). The trade winds blowing from east to west are very humid. The orographic interception of the moisture carried by these winds generates an orographic lift promoting the formation of clouds and rainfalls on windward slopes. Consequently, on the studied catchment, the MAR evolves from 2650 mm at 65 m asl to 4400 mm at the top of the catchment (400 m asl) (Fig. 1b). The soils are thus distributed along a climosequence. They formed from pyroclastic andesitic deposits of pumice lapilli type from 30,000 to 18,000 years BP (Fig. 2b) (Charlier et al., 2011; Colmet-Daage and Lagache, 1965; Crabit et al., 2016; Dagain, 1981; Sak et al., 2010; Samper et al., 2007) with plagioclase, pyroxene and volcanic glass as dominant weatherable minerals (Dagain, 1981; Ndayiragije and Delvaux, 2003; Sak et al., 2010; Samper et al., 2007). At MAR > 4000 mm, perhydrated Andosols (Fig. 1b) contain (Al, Fe)-humus, allophane and gibbsite as dominant secondary products. In particular, the abundance of large particles of gibbsite, developing as pseudomorphs of plagioclase and pyroxene, as well as clay-sized gibbsite, reflects strong desilication (Ndayiragije and Delvaux, 2003). These pseudomorphs occur in silt and fine sand fractions of weathered Bw horizon (Ndayiragije and Delvaux, 2003) as well as in andesitic clasts in bedrocks (Sak et al., 2010). At MAR < 4000 mm, allophane is the dominant clay mineral, while C and gibbsite contents slightly decrease (Colmet-Daage and Lagache, 1969). Halloysite and Fe oxide are abundant in the Nitisols that developed in the lowest parts of the catchment. All soils are strongly microaggregated (Dorel et al., 2000). The catchment is probably intensively cultivated below ~390 m asl since the late seventeenth century AD: at and below 250 m asl,

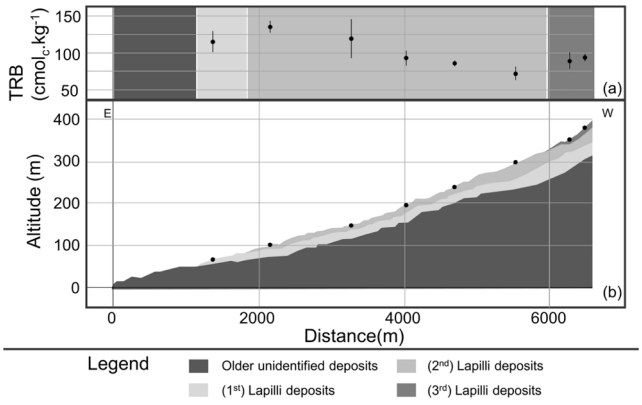

Fig. 2. (a) Evolution of the Total Reserve in Bases (TRB; Herbillon, 1986) along the soil climosequence; (b) schematic geological profile. Depth of the deposits are not scaled but enlarged to improve visualization.

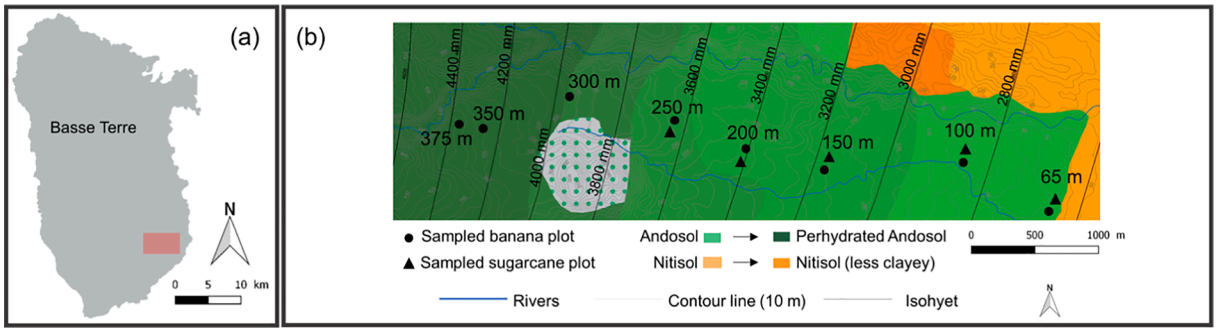

Fig. 1. (a) Location of the studied soil climosequence, Basse-Terre Island, Guadeloupe. (b) Location of sampling sites on the soil map figured out with isohyets (MAR black lines): banana (●), sugarcane (▲).

sugargane was long cropped at least since 1669 while banana cultivation started in 1976 (Doumenge, 1985). Sugarcane was never cropped above 250 m asl so that intensive cropping exclusively involved banana in the altitude range 250–390 m asl. At the top of the catchment, from ~390 m asl upslope, natural rainforest is protected in the National Park of Guadeloupe. Presently, croplands and forests cover 56.7% and 17.4% of the total surface, respectively. Intensive banana and sugarcane crops account for 60.1% and 11.4% of cultivated land, respectively.

3. Materials and methods

3.1. General sampling scheme

In the catchment, from ~390 m downslope, intensive cropping exclusively involves banana (≤375 m asl) and sugarcane (≤250 m asl) on a long term and historical basis. Food crops do occur, here and there, in vegetable gardens that shelter a complex diversity with a lack of historical data. So, we selected cultivated plots of banana and sugarcane, both of which are monocots equipped with active transporters for Si uptake (Henriet et al., 2006; Keeping et al., 2009).

Eight banana (BA) (*Musa acuminata*, Cavendish, group AAA, desert banana) and five sugarcane (SC) (*Saccharum officinarum*) cultivated plots were selected along a climosequence at 65, 100, 150, 200, 250, 300, 350, 375 m asl, and 65, 100, 150, 200, 250 m asl, respectively (Fig. 1b). The landscape is gently sloping, and the average slope is 6–7%. On each banana plot (except at 375 m), 18 plants were randomly selected at flowering stage. For each plant, we sampled the external part of the lamina at the center (100 mm width) of the antepenultimate leaf (leaf III) following the international standard set up for banana foliar diagnosis (Martin-Prével, 1980). Afterwards, three groups of 6 leaves were randomly constituted and mixed to obtain three composite samples for each site. Sugarcane leaves could not be sampled because the field study took place just after harvesting. In each plot, nine bulk topsoil samples (0–20 cm) were collected randomly, and combined into 3 composite samples, while six undisturbed moist topsoil samples were collected at field capacity using Kopecky cylinders to measure the bulk density. For comparison purpose regarding weathering and soil processes, a neighboring forest (FO) plot was selected at the top of the catchment (396 m asl), in which bulk and undisturbed topsoils were collected using the same sampling strategy. For reading facilities, each topsoil (0–20 cm) is identified through its plot name including the land use (BA, SC, FO) and altitude (m asl): BA65, SC65 to BA375 and FO396.

3.2. Basic soil analyses

Soil texture was determined by quantitative recovery of clay, silt and sand fractions after sonication and dispersion with Na^+ saturated resins without any previous oxidation of SOM (Rouiller et al., 1972). pH was measured in H_2O using 5 g : 25 ml suspensions. Phosphate retention was measured according to Blakemore (1983). Dark oxalate-extractable (o), dithionite-citrate-bicarbonate (DCB) extractable (d) and pyrophosphate-extractable (p) contents of Si, Al and Fe were determined in the respective extracts by inductively coupled plasma-atomic emission spectrometry (ICP–AES) following the methods compiled in Dahlgren (1994). Total (t) elemental concentrations were determined on soil samples by ICP-AES after fusion in Li-metaborate and Li-tetraborate at 1000 °C (Chao and Sanzolone, 1992). The indices t, o, d and p were used to qualify the respective element contents. Total C and N contents were determined by high temperature dry combustion using a Vario EL Cube elemental analyzer. Crystalline soil minerals were identified by X-ray diffraction (XRD) on powder soil (<2 mm) and oriented clay (<2 μm) samples using CuK_α radiation in a Bruker Advance diffractometer.

3.3. Weathering indices

The Total Reserve in Bases, TRB (cmol(+) kg^{-1}) sums up the total elemental contents of major alkaline and alkaline-earth cations, reflecting the reserve of weatherable minerals (Herbillon, 1986). The elemental $Si_t/(Al_t + Fe_t)$ atomic ratio and the Fe_d/Fe_t ratio were also used as indicators of the soil weathering stage (Barrett, 2001; Delvaux et al., 1989; Egli et al., 2001; Leigh, 1996). In addition, to estimate the extent of chemical alteration, three weathering indices were derived from analytical data, each oxide content being divided by its respective molecular mass:

Chemical Index of Alteration, $CIA = 100 \times Al_2O_3/(Al_2O_3 + CaO + Na_2O)$ (Nesbitt and Young, 1989).

Base Depletion Index, $BDI = (CaO + MgO + Na_2O + K_2O)/(Fe_2O_3 + Al_2O_3 + TiO_2)$ (Jien et al., 2016).

Parker Index, $PI = 100 \times (CaO/0.7 + MgO/0.9 + 2Na_2O/0.35 + 2K_2O/0.25)$, (Parker, 1970).

3.4. Thermogravimetric analyses

Thermogravimetric analysis (TGA) was used to estimate the content of gibbsite in the Mg^{2+}-saturated clay fraction previously treated with DCB (5–10 mg) (Ndayiragije and Delvaux, 2003). TGA was carried out with a Mettler Toledo TGA/SDTA 851e in a flowing nitrogen atmosphere (50 ml min^{-1}) from 30 °C to 1000 °C with a heating rate of 10 °C min^{-1}, using gibbsite from Alcoa® Company <https://www.alcoa.com> for calibration purposes. The thermal events were interpreted by plotting the derivatives of the TGA curves.

3.5. Specific Si extractions

$CaCl_2$. $CaCl_2$-extractable Si content ($CaCl_2$-Si) is considered to assess the bioavailable Si pool in soils (Haysom and Chapman, 1975; Sauer et al., 2006). We carried out a 6 h to 64 days kinetic extraction using a solid:liquid ratio 5 g:50 ml (0.01 M $CaCl_2$) in 100 ml polyethylene cups shaken at 25 °C following the procedure of Li et al. (2019). The Si concentration in the $CaCl_2$ extract (diluted 10 times and neutralized by 50 μl of a 15 M HNO_3 solution) was measured by ICP-AES.

Na_2CO_3. Na_2CO_3-extractable Si content was determined to assess phytolithic Si (PhSi) in soils (DeMaster, 1981; Koning et al., 2002; Sauer et al., 2006). We carried out a kinetical extraction (DeMaster, 1981). Forty milligrams of soil sample (<2 mm) were mixed with 40 ml of 0.1 M Na_2CO_3 at 85 °C during 7 h. One milliliter of solution was collected after 15, 60, 120, 180, 240, 300, and 360 min, diluted with 9 ml of deionized water and acidified with 50 μl of Suprapur HNO_3. Si, Al, Fe, and Mg concentrations were measured at each time by ICP-AES. According to DeMaster (1981), the intercept of the linear part of the time release of Si estimates the amorphous Si (ASi) pool. Na_2CO_3 kinetical extractions were performed on soil samples respectively untreated and pretreated using dark oxalate extraction (Blakemore, 1981), immediately followed by a rinsing using $CaCl_2$ 0.01 M (Sauer et al., 2006) to remove residual dissolved Si (DSi). Dark oxalate buffered at pH 3 dissolves organo-mineral associations (OMA), short range ordered (SRO) pedogenic silicates (PSi) (allophane and imogolite), adsorbed forms of Si, and Fe oxide (ferrihydrite) (Parfitt and Childs, 1988; Wada, 1989, 1977), and possibly poorly crystalline Al hydroxide (Huang et al., 2002). The dark oxalate pretreatment was carried out to bring the ASi pool as close as possible to the PhSi pool by removing mineral SRO silicates from the soil materials. The ASi content of untreated soil is named Na_2CO_3-Si whereas the PhSi content of oxalate-treated soil is ox-Na_2CO_3-Si.

Heavy liquid separation. This physical extraction was carried out on one composite sample for each plot. Following Henriet et al. (2008b), the silt fraction was recovered after sonication and dispersion with Na^+ saturated resins without any previous oxidation of SOM (Rouiller et al., 1972), then treated with H_2O_2 and DCB. An additional dispersion using Na^+-saturated resins (Rouiller et al., 1972) was carried out overnight to discard any clay contamination. The silt fraction was then divided into light and heavy components, through a series of heavy liquid

separations, using a Na polytungstate solution with a density of 2.3 g cm^{-3} (adapted from Kelly, 1990). Each silt fraction was mixed with 20 ml of Na polytungstate and centrifuged at 4000 rpm for 10 min. After centrifugation, the supernatant containing floating particles was carefully removed with a pipette and collected on a Teflon filter (2 μm). The operation was repeated until the supernatant was clear. The filter was then rinsed with 1 M HCl and washed with deionized water. The light fraction was submitted to a XRD analysis, and to a total elemental analysis by fusion in Li-metaborate and Li-tetraborate at 1000 °C. Extracted Si, Al, Fe, and Mg contents were determined by ICP-AES. XRD data were further used to quantify the components of the light fraction using the SIROQUANT © quantitative XRD software (version 2.5). In fact, we did not count the phytolithic particles on microscope images because of the substantial occurrence of other minerals in the light fractions. We further calculated the content of phytolithic Si from that of PhSi particles as estimated after XRD quantification, in order to compare it with the Si concentration measured in $CaCl_2$ and Na_2CO_3 extracts. A phytolith mean water content of 10% was assumed (equivalent to 0.37 mol of H_2O for 2 mol of SiO_2) (Alexandre et al., 1997; Meunier et al., 2014). The PhSi content as assessed by XRD after heavy liquid (*hl*) separation is named XRD-*hl*PhSi.

3.6. Foliar analysis

Banana leaf samples were thoroughly washed with 70% ethanol in order to remove eolian pollution. They were dried at 70 °C for four days and then grinded. Elemental analysis was carried out after calcination at 450 °C for 1 day and fusion in Li-metaborate + Li-tetraborate at 1000 °C (Chao and Sanzolone, 1992), followed by the pellet dissolution in 15% HNO_3. Nutrient and Si concentrations were measured by ICP-AES.

3.7. Hypotheses and statistical analyses

All statistical analyses were conducted with the R programing language (version 3.4.4). First, differences of means were tested with a *t*-test with the pairwise.t.test function. Next, we explored linear relationship among soil Si pools ($CaCl_2$-Si, Na_2CO_3-Si, ox-Na_2CO_3-Si, total Si, XRD-*hl*PhSi) and the three hypothesized possible influencing parameters: MAR, TRB (reflecting soil weathering stage), and pH. To do this, we used the *lm* function of the R programing language (Eq. (1)).

$$Si_{pool}\ a + bMAR + cTRB + dpH$$

4. Results

4.1. Soil properties and constituents

At a given altitude, soil properties in banana (BA) and sugarcane (SC) plots were similar (Tables S1–S3). Therefore, we considered the whole data set as based on six repetitions per altitude level, whatever the crop, as presented in Table 1. Soil texture was clay loam to clay. With increasing altitude, clay content and TRB tended to decrease below 38% and 100 cmol(+) kg^{-1}), respectively, bulk density decreased (0.8–0.5 g cm^{-3}) while C content increased from 42 to 97 g kg^{-1} in cultivated topsoils, reaching 155 g kg^{-1} under forest. The narrow ranges of the elemental $Si_t/(Al_t + Fe_t)$ atomic ratio and Fe_d/Fe_t ratio were 1.0–0.8 and 0.52–0.47, respectively. Selective extraction data reveal the presence of allophanic substances (80–161 g kg^{-1}), Al-humus components (Al_p: 6.7–12.3 g kg^{-1}), and ferrihydrite (Fe_o: 10.9–18.4 g kg^{-1}). Allophanic substances had a low Si/Al atomic ratio (0.51–0.65), which denotes their aluminous composition close to that of imogolite (Si/Al = 0.5). Imogolite, however, was not identified in the clay fractions in contrast to its occurrence in weathered soil horizons developed from recent (≈500 yr old) andesitic ash on the western flank of the volcano at 1000 m asl and MAR ≥ 4500 mm (Jongmans et al., 1994). Oxalate extractable Fe content (Fe_o), referring to SRO Fe oxide and Fe-humus, represented 23–29% of total free iron below 300 m asl, and 39 to 49% above that level, in relation to larger C contents. Phosphate retention (P ret, Table 1) was above 95% whatever the altitude.

XRD data performed on bulk soil (<2 mm) (Fig. S1) revealed the occurrence of gibbsite, quartz, tridymite and cristobalite as well as trace amounts of halloysite and possibly 2:1:1 phyllosilicate as previously

Table 1
Selected topsoil (0–20 cm) properties as measured on the fine earth fraction (<2 mm), except for gibbsite content measured on DCB treated, Mg^{2+}-saturated clay fractions (<2 μm) at each altitude level: particle size analysis, bulk density, Total Reserve in Bases (TRB), elemental $Si_t/(Al_t + Fe_t)$, Fe_d/Fe_t and Fe_o/Fe_d atomic ratios, contents of organic C and allophane, $Si_o/(Al_o\text{-}Al_p)$ atomic ratio, the intensity of the 002 XRD reflection at 0.485 nm ($I_{0.482}$), clay-sized gibbsite content and P retention (P ret). The average values are computed from individual values as determined on six composite topsoil (0–20 cm) samples collected in banana (3) and sugarcane (3) plots at 65, 100, 150, 200, and 250 m, but on three composite samples in banana plots at 300, 350, and 375 m, and at 396 m under forest. Different lowercase letters express significant differences at $p < 0.05$ level for TRB, $Si_t/(Al_t + Fe_t)$, Fe_d/Fe_t, Fe_o/Fe_d, C, allophane content and $Si_o/(Al_o\text{-}Al_p)$. Differences were tested with a *t*-test with the pairwise.t.test function of the R programming language.

Altitude	Particle size analysis (%)			Bulk density	TRB	$Si_t/(Al_t + Fe_t)$[a]	Fe_d/Fe_t	Fe_o/Fe_d	C	Allophane[b]	$Si_o/(Al_o\text{-}Al_p)$[c]	$I_{0.482}$[e] (<2 mm)	Gibbsite(<2 μm)	P ret
m	Clay	Silt	Sand	g cm^{-3}	$cmol_c$ kg^{-1}				g kg^{-1}	g kg^{-1}		a.u.	g kg^{-1}	%
65	39.2	48.0	12.8	0.82	114 abc	1.01 a	0.52 a	0.27 ab	42.3 a	95 ab	0.61 a	4	31.0	96
100	48.7	32.5	18.8	0.78	134 a	0.90 b	0.49 a	0.27 ab	49.9 ab	161 c	0.55 a	8	72.7	97
150	40.6	36.5	22.9	0.74	118 ab	0.80 cd	0.50 a	0.27 ab	55.0 b	122 a	0.65 a	25	101.1	98
200	30.2	46.4	23.4	0.73	92 cd	0.79 cd	0.51 a	0.29 a	54.6 b	104 ab	0.62 a	26	112.9	96
250	18.4	45.9	35.7	0.70	85 d	0.79 c	0.53 a	0.23 b	48.8ab	73 b	0.65 a	31	101.8	96
300	37.1	41.0	21.9	0.73	71 d	0.78 cd	0.53 a	0.27 ab	51.6 ab	95 ab	0.54 a	40	112.7	96
350	34.1	47.6	18.3	0.57	88 bcd	0.87 bcd	0.48 a	0.39 ac	78.2 c	85 b	0.61 a	59	103.6	96
375	35.5	38.2	26.3	0.51	93 bcd	0.91 bcd	0.47 a	0.49 d	97.0 d	80 b	0.52 a	36	101.9	97
396[d]	34.0	44.9	21.1	0.48	85 d	0.94 bcd	0.54 a	0.41 c	155.0 e	30 d	0.68 b	19	58.5	98

[a] Computed from total elemental contents Si_t, Al_t and Fe_t (Table S2).
[b] Allophanic substances; estimated according to Parfitt and Wilson (1985), using Si_o, Al_o and Al_p contents (Table S1).
[c] Computed from Si_o, Al_o and Al_p contents (Table S1).
[d] Rainforest (National Park of Guadeloupe).
[e] As measured on XRD spectra performed on powdered bulk topsoil (<2 mm) samples.

identified (Ndayiragije and Delvaux, 2003). Remarkably, the intensity of the d_{002} XRD reflection at 0.485 nm ($I_{0.482}$) typical for gibbsite first increased with increasing altitude up to 350 m asl, then decreased upslope, similarly to the content of clay-sized gibbsite as estimated by TGA (Table 1). Comparing the XRD data performed on the clay fractions (<2 μm) extracted from BA350 and FO396 topsoils (Fig. 3) confirmed the presence of clay-sized gibbsite and above-cited silica oxides, as well as the occurrence of halloysite, but in trace amounts. Moreover, the d_{002} XRD reflection of gibbsite at 0.482 nm ($I_{0.482}$) was much less intense in FO396 than in BA350 whatever the treatment, as also figured out in Table 2. Remarkably, gibbsite in FO396 was much less stable upon heating as compared to BA350 since the reflection at 0.482 nm virtually disappears at 300 °C in the former, while it was attenuated in the latter, as compared to the intensity of that reflection registered at room temperature (Table 2).

4.2. XRD and total elemental composition of the *hl*PhSi particles

XRD data performed on *hl*PhSi particles, extracted after heavy liquid (*hl*) separation, revealed the occurrence of cristobalite, tridymite, and gibbsite particles (Fig. S2), which could not be separated from phytoliths because of their respective densities of 2.32–2.36, 2.25–2.28 g cm^{-3}, and 2.34 g cm^{-3} (Huang et al., 2002; Monger and Kelly, 2002), very close to that of phytoliths (~2.3 g cm^{-3}).

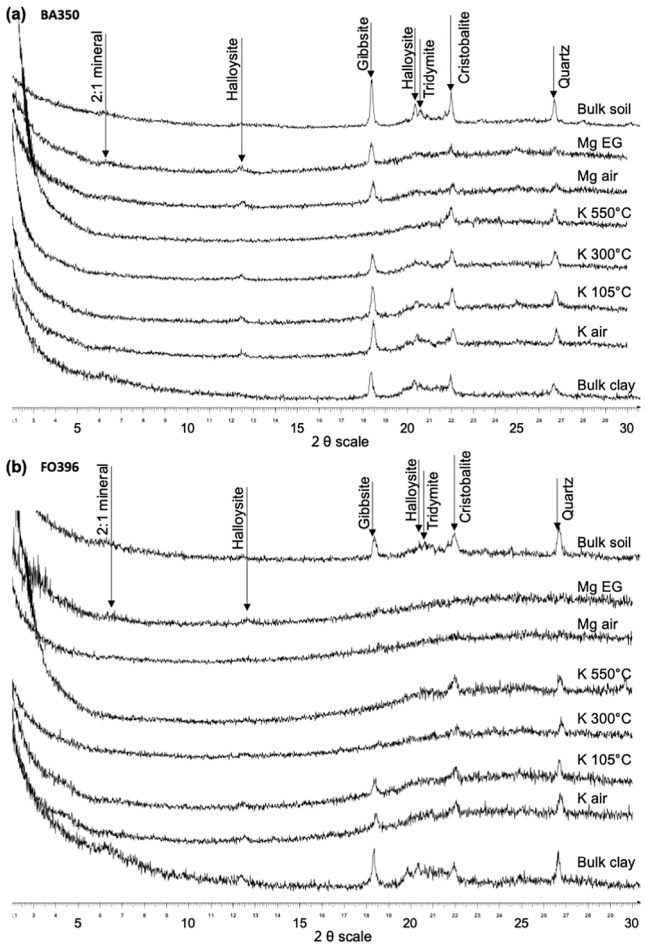

Fig. 3. X-ray diffraction (XRD) patterns performed on the bulk topsoil (<2 mm, non-oriented powder) and on the clay fractions (<2 μm, oriented) extracted from samples BA350 (a) and FO396 (b). XRD on oriented clays were performed bulk and saturated with either K^+ or Mg^{2+}, at air room temperature (20 °C) after formamide intercalation, overnight ethylene–glycol saturation (EG), as well as after heating at 110, 300 and 550 °C (4 h).

Table 2
Intensity of the XRD reflection d_{002} of gibbsite at 0.482 nm ($I_{0.482}$) as measured in arbitrary units (a.u.) on XRD patterns performed on oriented clays for (a) BA350 and FO396, as shown in Fig. 5.

Sample	Mg^{2+} 20°	Mg^{2+} EG	K^+ 20°	K^+ 105°	K^+300°	K^+550°
BA350	42	30	62	58	40	0
FO396	0	0	38	30	2	0

Loss on ignition of *hl*PhSi particles ranged between 3.7 and 15.1% irrespective of altitude (Table 3). The ranges of SiO_2 and Al_2O_3 concentrations were 70.3–92.2%, and 3.3–15%, respectively (Table 3). The Si/Al atomic ratio of *hl*PhSi particles amounted to 30 at 375 m asl, but ranged between 5 and 13 in BA topsoils, and between 9 and 15 in SC topsoils. The concentrations of other oxides were below 1%. The elemental composition of *hl*PhSi particles did not show any trend in relation to altitude.

The quantification of phytoliths, tridymite, cristobalite, and gibbsite with SIROQUANT software showed that the percentage of phytoliths in heavy liquid extracts varied widely from one sample to another (Table 4). It ranged from 12.7 to 63.8% in BA topsoils and from 10 to 76.2% in SC topsoils.

4.3. Si pools in soils and leaf Si content

As for soil properties, Si concentrations in soil were similar at a given altitude between neighboring BA and SC plots (Table S4). We thus considered the whole data set as based on six repetitions per altitude level. The Na_2CO_3-Si content ranged between 10.3 and 12.6 g kg^{-1} irrespective of altitude. The XRD-*hl*PhSi content increased with altitude from 6.05 to 53.45 g kg^{-1}. In contrast, Si_t, $CaCl_2$-Si and ox-Na_2CO_3-Si contents significantly decreased with increasing altitude (Table S4): Si_t from 179 to 142 g kg^{-1}, $CaCl_2$-Si from 66 to 14 mg kg^{-1}, and ox-Na_2CO_3-Si from 7.7 to 2.0 g kg^{-1}. The banana leaf Si content ranged between 3.81 and 5.30 g kg^{-1}, regardless of altitude. Except at the lowest altitude level (65 m), XRD-*hl*PhSi was invariably higher than ox-Na_2CO_3-Si: from 1.5 times at 100 m to 11 times higher at 375 m.

4.4. Methodological considerations

Physical extraction of phytoliths. The heavy liquid separation extracted phytoliths, but also tridymite, cristobalite, and gibbsite (Fig. S2). Tridymite and cristobalite have a specific gravity (2.2–2.3 g cm^{-3}) close to that of phytolith (2.3) unlike quartz (2.53–2.65) (Monger and Kelly, 2002), and slightly below that of gibbsite (2.34 g cm^{-3}). Phytolith particles were not counted (Kelly, 1990) due to the substantial occurrence of tridymite, cristobalite, and gibbsite. Quantitative assessment from XRD data showed that phytolith content in heavy liquid extracts ranged from 10 to 76.2%.

Chemical extraction of phytoliths. Na_2CO_3–Si values as deduced from the *DeMaster* procedure (DeMaster, 1981) were as high as 10.0–14.2 g kg^{-1} (Table S4), because of the release of structural Si from the alkaline dissolution of allophanic constituents (Wada, 1989). Probably, minor quantities of adsorbed Si could have been released from secondary oxides (Jones and Handreck, 1963), particularly SRO Fe oxide (Delstanche et al., 2009) and allophanic substances (Harsh et al., 2002; Wada, 1989). After the dark oxalate extraction of SRO aluminosilicates (Wada, 1989), SRO Fe and Al oxides (Bigham et al., 2002; Huang et al., 2002), and possibly adsorbed Si if any, ox-Na_2CO_3–Si markedly decreased to 2.0–7.9 g kg^{-1} (Table S4). However, Al content in the Na_2CO_3 extract after dark oxalate pretreatment was very high (5.2–8.5 g kg^{-1}, Table S4). We thus tentatively attribute ox-Na_2CO_3–Si to phytolithic silicon, and ox-Na_2CO_3–Al to SRO Al oxide and/or microcrystalline gibbsite (Huang et al., 2002), as further discussed in next sections.

Table 3
Elemental composition and ignition loss of the particles extracted from topsoil samples (0–20 cm) by heavy liquid separation for each cultivated plot at each altitude. The plot name includes the land use (BA, SC, FO) and altitude (m asl).

Plot	Al_2O_3	CaO	Fe_2O_3	K_2O	MgO	Na_2O	SiO_2	TiO_2	Ignition loss	Si/Al
					%					atomic ratio
BA65	9.52	0.19	0.58	0.13	0.12	0.28	78.72	0.18	10.29	8.99
SC65	6.27	0.14	0.51	0.13	0.09	0.35	86.63	0.18	5.70	15.03
BA100	15.04	0.14	0.88	0.13	0.14	0.35	69.49	0.23	13.59	5.02
SC100	11.57	0.15	0.74	0.13	0.10	0.34	76.53	0.21	10.22	7.19
BA150	12.68	0.16	1.03	0.18	0.13	0.20	70.32	0.19	15.10	6.03
SC150	7.24	0.11	0.58	0.13	0.08	0.19	82.57	0.15	8.95	12.40
BA200	10.84	0.14	0.95	0.11	0.09	0.35	70.67	0.19	16.66	7.09
SC200	6.67	0.14	0.66	0.10	0.06	0.10	81.84	0.14	10.28	13.34
BA250	6.49	0.20	0.70	0.15	0.12	0.15	81.32	0.14	10.74	13.6
SC250	9.47	0.14	0.89	0.19	0.12	0.25	79.99	0.20	8.76	9.19
BA300	7.84	0.14	0.66	0.04	0.12	0.20	83.82	0.16	7.02	11.63
BA350	12.71	0.35	0.69	0.15	0.13	0.20	74.65	0.15	10.96	6.39
BA375	3.29	0.21	0.28	0.10	0.06	0.09	92.24	0.09	3.65	30.50

Table 4
Portion of each component of the particles extracted by heavy liquid separation for each plot at each altitude (BA: banana; SC: sugarcane) as estimated with the SIROQUANT © quantitative XRD software (version 2.5). The plot name includes the land use (BA, SC, FO) and altitude (m asl).

Plot	Total (*hl* particles[1])	Phytolith		Cristobalite		Tridymite		Gibbsite	
	g kg^{-1}	%	g kg^{-1}	%	g kg^{-1}	%	g kg^{-1}	%	g kg^{-1}
BA65	47.59	12.7	6.04	31.4	14.94	52.1	24.79	3.8	1.81
SC65	60.63	10.0	6.06	51.8	31.41	36.5	22.13	1.7	0.91
BA100	66.6	38.5	25.64	29.7	19.78	25.2	16.78	6.7	4.13
SC100	60.69	27.9	16.93	37.8	22.94	28.9	17.54	5.3	2.79
BA150	61.69	24.7	15.24	24.3	14.99	43.3	26.71	7.8	4.63
SC150	46.39	38.0	17.63	15.5	7.19	40.8	18.93	5.6	2.51
BA200	51.71	43.3	22.39	12.2	6.31	37.0	19.13	7.4	3.67
SC200	46.62	76.2	35.52	2.4	1.12	18.9	8.81	2.4	1.07
BA250	40.07	65.6	26.29	3.7	1.48	28.8	11.54	1.9	0.76
SC250	50.97	36.1	18.40	12.4	6.32	46.0	23.45	5.5	2.80
BA300	71.3	38.0	27.09	12.4	8.84	45.2	32.23	4.4	3.14
BA350	91.2	51.6	47.06	9.6	8.76	23.9	21.80	14.9	13.59
BA375	83.78	63.8	53.45	3.8	3.18	29.0	24.30	3.4	2.85

[1] hl particles are the extracted particles with the heavy liquid extraction method.

5. Discussion

5.1. Andic properties

The sodium fluoride field test (Fieldes and Perrot, 1966) gave a rapid, strong and positive response indicating the occurrence of allophane and/or organo-aluminum complexes in both topsoil and subsoil whatever the altitude. Analytical data revealed the strong expression of andic properties in all studied topsoils. The values of bulk density ≤0.82 g cm^{-3} (Table 1), phosphate retention ≥96% and [Al_o + ½Fe_o] ≥ 2% (Fig. 4) indeed fulfill the diagnostic criteria that are required for andic properties (IUSS Working Group WRB, 2014)

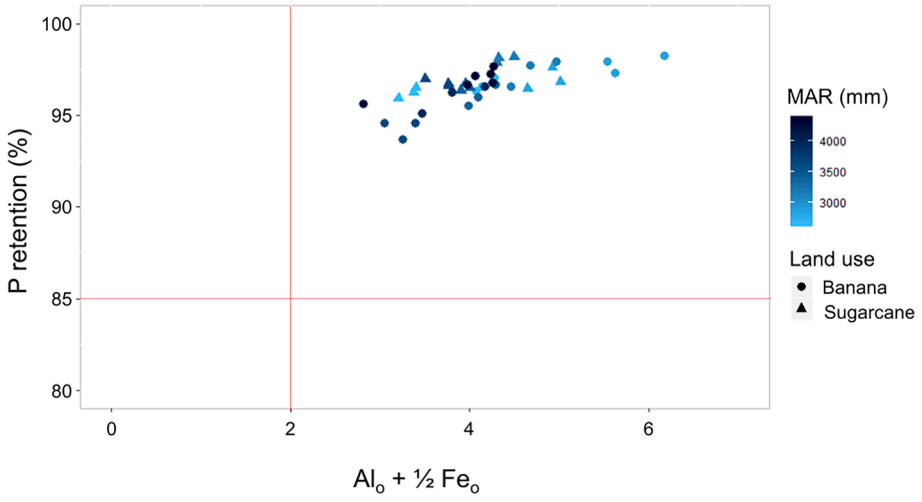

Fig. 4. Plot of P retention against Al_o + ½ Fe_o ratio. The color of each point reveals the MAR (Mean Annual Rainfall) level. Red lines show the lower limits of each parameter for Andic properties.

regardless of rainfall and altitude. Andic properties were previously diagnosed in the whole A-Bw horizons assemblage, all horizons having clay loam to clay textures (Vander Linden, 2019).

5.2. Soil weathering stage

Given the values of the elemental $Si_t/(Al_t + Fe_t)$ atomic ratio (1.0–0.8) and Fe_d/Fe_t (0.52–0.47), all soils had reached an advanced stage of mineral weathering and desilication, in particular above 150 m asl where TRB was below 100 $cmol_c\ kg^{-1}$. Fig. 5 reveals the strong correlation between TRB and other weathering indices (PI, CIA, BDI), and illustrates the impact of rainfall on weathering stage: the most weathered soils occurred at the wettest positions in the climosequence. Furthermore, the comparison of our studied materials to other topsoils (0–20 cm) from the same weathering sequence (Henriet et al., 2008a), and to fresh andesitic ash materials from the same volcanic area (Cabidoche et al., 1987; Opfergelt et al., 2012; Sak et al., 2010; Samper et al., 2007) (Fig. 6) supports that the studied topsoils have reached an advanced weathering stage neighboring the one of ferrallitic domain. The distribution of the values of TRB and $Si_t/(Al_t + Fe_t)$ atomic ratio in the same set of samples (Fig. S3) further illustrates the clear distinction between fresh or little weathered andesitic materials from the same area and the soil materials both studied here and previously analyzed (Henriet et al. 2008a). Low $Si_t/(Al_t + Fe_t)$ values indicate strong desilication, which is also revealed by large gibbsite contents in both the bulk soil (Table 1, Fig. S1) and the clay fraction (31–113 g kg^{-1} clay) (Table 1; Fig. 3). Abundant gibbsite is indeed a major indicator of strong desilication. Actually, gibbsite occurs in soils of any age whenever Si is in low supply, hence under strong leaching (Churchman and Lowe, 2012). Where there is a gradation in the extent of leaching, often because of a change in altitude change, gibbsite occurs in the most heavily leached soils whereas 1:1 phyllosilicates are dominant secondary minerals where there is a lesser degree of leaching (Churchman and Lowe, 2012; Herbillon et al., 1981; Huang et al., 2002; Nieuwenhuyse and van Breemen, 1997; Norfleet et al., 1993). Unlike generally accepted, clay content did not increase with increasing weathering, clay content and TRB being here positively correlated (r = +0.64). Underestimating clay content through poor dispersion could be discarded, except in BA200 (Table S3) since the Na-resin procedure proved to be efficient in andic and ferrallitic materials (Bartoli et al, 1991; Delvaux et al., 1989). Though clay-sized particles can be aggregated into very stable secondary particles about 5–300 μm in size with increasing weathering (Cornell and Schwertmann, 2003), we privilege two hypotheses here: (i) clay dissolution and (ii) limited clay neoformation. (i) Clay-sized phyllosilicates and allophanic materials (Dahlgren and Saigusa, 1994) readily act as proton consumers in soils depending on pH buffering environment (van Breemen et al., 1983). They are the major, if not exclusive, H^+-consumers once the reserve of primary minerals is exhausted (van Breemen et al., 1983). Moreover, clay dissolution is strongly enhanced by SOM compounds acting as proton donors and complexing agents, as observed with increasing weathering in both tropical (Fritsch et al., 2011) and temperate conditions (Brahy et al., 2000). (ii) On the other hand, limited clay neoformation would be enhanced in a perudic environment through the intense leaching of silica and other solutes from mineral dissolution. Thus, in our climosequence, TRB, PI, BDI globally decrease with increasing altitude, SOM content and rainfall. These trends suggest that such environmental conditions could promote both the dissolution and limited neoformation of clay-sized particles while weathering increases.

5.3. Soil secondary products

In addition to soil organic matter (SOM), the main secondary products are Al-rich allophane, Fe and Al hydroxides as well as (Fe, Al)-humus compounds. The formation of aluminous allophane is due to the leaching of silica (Wada, 1977, 1989; Harsh et al., 2002). At the highest, wettest sites, SOM accumulation hampers the crystallization of Fe oxides (Bigham et al., 2002) as revealed by the highest proportion of poorly crystalline and organically-bound Fe forms. Similarly, SOM accumulation in the forest soil has inhibited allophane synthesis and gibbsite formation likely through antiallophanic and antigibbsitic effects (Shoji et al., 1993; Ndayiragije and Delvaux, 2003; Churchman and Lowe, 2012), respectively, which account for the competition for available Al between mineral formation and complexation by organic compounds. The lowest allophane content ($\leq$30 g kg^{-1}) is indeed measured at the top of the catchment area in FO396 sample. In addition to Al-rich allophane, strong desilication and SOM accumulation have thus promoted the formation of a continuum Al-humus – poorly crystalline Al hydroxide – gibbsite as predicted earlier (Huang et al., 2002) and reported recently (Anda and Dahlgren, 2020). Increasing perudic conditions have driven this continuum towards the Al-humus pole, limiting the synthesis of gibbsite in addition to that of allophane, the antigibbsitic and antiallophanic effects being cumulated in the forest topsoil (FO396). In the pair of samples considered in Fig. 3 and Table 2, the allophane content in FO396 is indeed ~3 times lower than that of BA350 whereas the SOM content in FO396 is twice as high as in BA350 (Table 1). Since gibbsite content decreases at highest altitude (Table 1), the lower $I_{0.482}$ in FO396 (Fig. 3, Table 2) further illustrates the antigibbsitic effect due to SOM accumulation. In addition, the thermal instability of the gibbsitic component in FO396 may reveal a lower crystallinity and/or smaller particle size of Al hydroxide in tsFO396 due to SOM accumulation (Mehta et al., 1992). Furthermore, litter biodegradation alters the original gibbsite structure into microcrystalline gibbsite, less crystalline Al hydroxide and organo-hydroxy-aluminum complexes through the dissolution of gibbsite surfaces and concomitant precipitation of short-range-order or amorphous phases (Heckman et al., 2013). Here, the SRO Al oxide pool likely contains poorly crystalline Al hydroxide particles as defined by Huang et al. (2002), who reported SRO Al oxide contents ranging from 5 to 10 g kg^{-1} in Brazilian ferrallitic soils as assessed by dark oxalate extraction. We could not

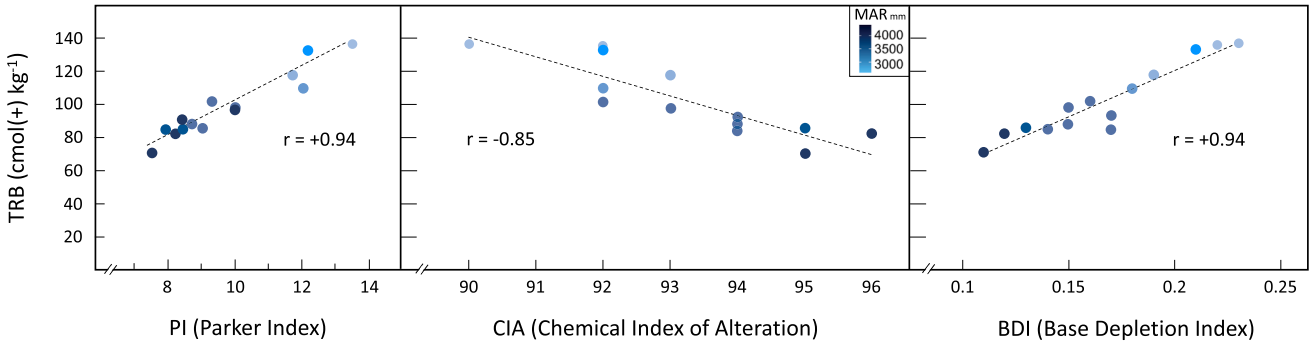

Fig. 5. Plots of TRB against PI, CIA and BDI for the studied topsoils (0–20 cm). The color of each point reveals the MAR (Mean Annual Rainfall) level.

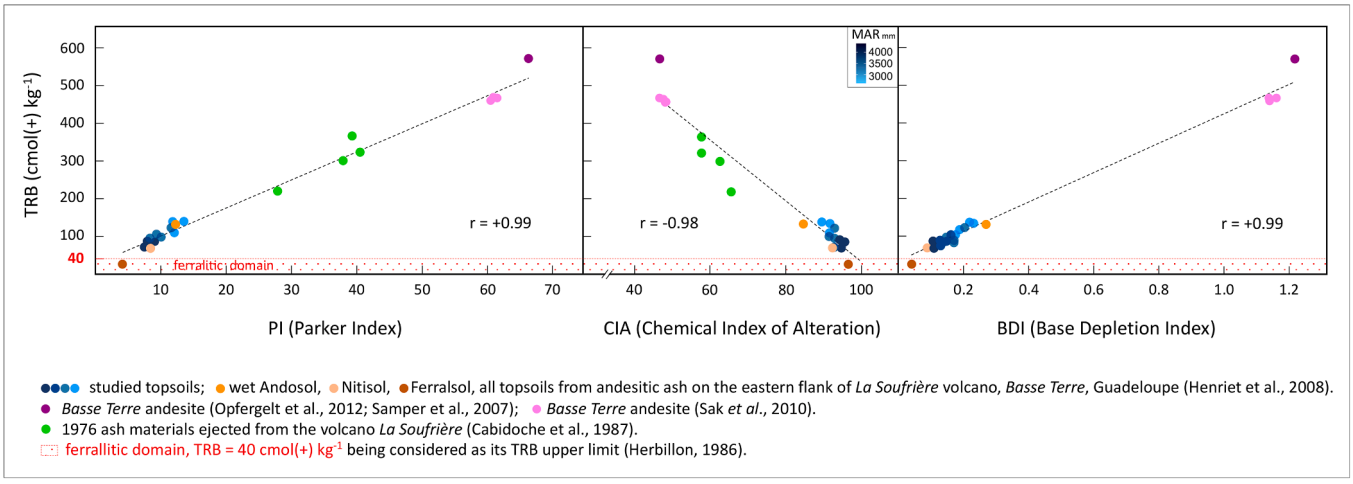

Fig. 6. Plots of TRB against weathering indices PI, CIA and BDI in the studied topsoils (0–20 cm), for which the color of each point reveals the MAR (Mean Annual Rainfall) level, as well as in other topsoils (0–20 cm) from the same weathering sequence (Henriet et al., 2008), and in fresh andesitic ash materials from the same volcanic area (Cabidoche et al., 1987; Opfergelt et al., 2012; Sak et al., 2010; Samper et al., 2007).

quantify the content of poorly crystalline Al hydroxide because of the presence of allophanic substances of unknown Si/Al ratio. Since large particles of gibbsite appeared as pseudomorphs of plagioclase and pyroxene in neighboring perhydrated Andosols (Ndayiragije and Delvaux, 2003), we hypothesize that there are two pathways for the formation of gibbsite in these soil materials: (i) direct formation of gibbsite *in situ* as pseudomorphs (Ndayiragije and Delvaux, 2003), and (ii) an indirect formation, not *in situ*, but through a stage of poorly crystalline, clay-sized Al hydroxide (Huang et al., 2002).

5.4. Climatic controls on mineral neoformation, base saturation and fate of DSi

Mineral synthesis. The climatic controls on mineral synthesis thus resulted in the formation of Al-rich allophane, poorly crystalline Al hydroxide, gibbsite and Fe oxide whereas the relative importance of (Al, Fe)-humus complexes increased in the soils at the wettest sites. The most significant expressions of these climatic controls are the strong desilication and the increase in gibbsite content in both the bulk soil and the clay fraction at MAR > 3000 mm, concomitantly to the abrupt decrease in TRB from 134 to 114 to 93–71 $cmol_c\ kg^{-1}$.

Base saturation and buffering capacity. Soil ion exchange properties are controlled by a combination of weathering, leaching intensity and soil constituents (Chadwick et al., 2003). At MAR > 3000 mm, despite the abundant precipitation, the sum of exchangeable base cations (16.9–3.8 $cmol_c\ kg^{-1}$), base saturation (36–7%) and pH (6.5–5.1) show well-defined trends along the rainfall gradient (Fig. 7) as observed earlier (Chadwick et al., 2003; Henriet et al., 2008a). Average base saturation is invariably below 36% and is lowest (7–22%) in the wettest sites where the sum of exchangeable base cations is particularly low (4–10 $cmol_c\ kg^{-1}$). The loss of buffering capacity at high rainfall directly resulted from mineral weathering and the removal of base cations, and it led to a steep decline in effective cation exchange capacity and base saturation, despite the soils under banana cultivation are fertilized and limed. Actually, N and K fertilizer management in these perhydrated Andosols under intensive banana cropping is particularly acute since it requires frequent applications of small fertilizer doses to reduce nutrient losses through intense leaching (Godefroy and Dormoy, 1984; Ndayiragije and Delvaux, 2004). In addition, it should be noted that the only case of phosphorus deficiency in intensive banana plantations worldwide was reported in these perhydrated Andosols, due to P fixation on Al oxide surfaces (Lacoeuilhe and Godefroy, 1971). Though the soil buffering capacity has been exhausted for base cations, the release of plant available Si might has been "buffered" to some extent through the biological cycling of Si, which may alleviate natural soil desilication (Lucas et al., 1993), and theoretically to Si adsorption on oxide surfaces (Jones and Handreck, 1963), which should, however, be negligible here according to calculations using previous experimental data (Delstanche et al., 2009).

Fate of DSi. Increasing water availability increases the Si uptake by plants in dry conditions (Blecker et al., 2006; Katz et al., 2013) whereas it reaches maximum values as demonstrated experimentally in optimal conditions of water uptake (Henriet et al., 2006). Besides, plant transpiration plays a major role in plant silicon accumulation and distribution into different organs (Henriet et al., 2006). Here, under perhumid conditions, the low evapotranspiration negatively impacts plant Si accumulation and leaf biosilicification, despite the presence of residual weatherable silicate minerals, a source of DSi (de Tombeur et al., 2020). Moreover, the synthesis of secondary products majorly leads to the formation of aluminous phases involving Al-humus, poorly crystalline Al hydroxide, gibbsite and aluminous allophanic substances, as discussed here above. The pool of DSi in drainage waters is thus here a major sink of Si in the soil–plant system, in addition to neoformed aluminosilicate and plant phytolith (Li et al., 2020a). From a global perspective, the accumulation of Si by plants is therefore low under arid conditions, reaches a maximum under optimal conditions of evapotranspiration as well as water and Si availability, but drops under perhumid conditions due to the export of DSi, low bioavailability of Si and poor evapotranspiration.

5.5. Rainfall strongly impacts the pools of plant available Si and phytoliths

The perudic environmental framework offers the opportunity of deciphering the respective impacts of rainfall, soil weathering stage (TRB) and pH on the pools of bioavailable Si and phytoliths in soil. Linear models were realized using the *lm* function of the R programing language (Eq 1). From Table S5, these models showed that MAR was the only parameter that significantly explains the different Si pools ($CaCl_2$-Si $p < 0.001$, Na_2CO_3-Si $p < 0.05$, ox-Na_2CO_3-Si $p < 0.001$, XRD-*hl*PhSi $p < 0.003$, and total Si $p < 0.001$). In contrast, TRB and soil pH did not explain the differences in Si pools ($p > 0.05$). From these observations, we plotted Si_t, $CaCl_2$-Si, Na_2CO_3-Si, ox-Na_2CO_3-Si, XRD-*hl*PhSi contents in soils and leaf Si content against MAR (Fig. 8). The correlation was particularly strong with the first four variables (r ranging from −0.82 to −0.94) and the fifth one (r = +0.89). XRD-*hl*PhSi content increased with increasing MAR (r = +0.89) (Fig. 8e). In contrast, Si_t, $CaCl_2$-Si, Na_2CO_3-Si and ox-Na_2CO_3-Si and leaf Si contents decreased with increasing MAR

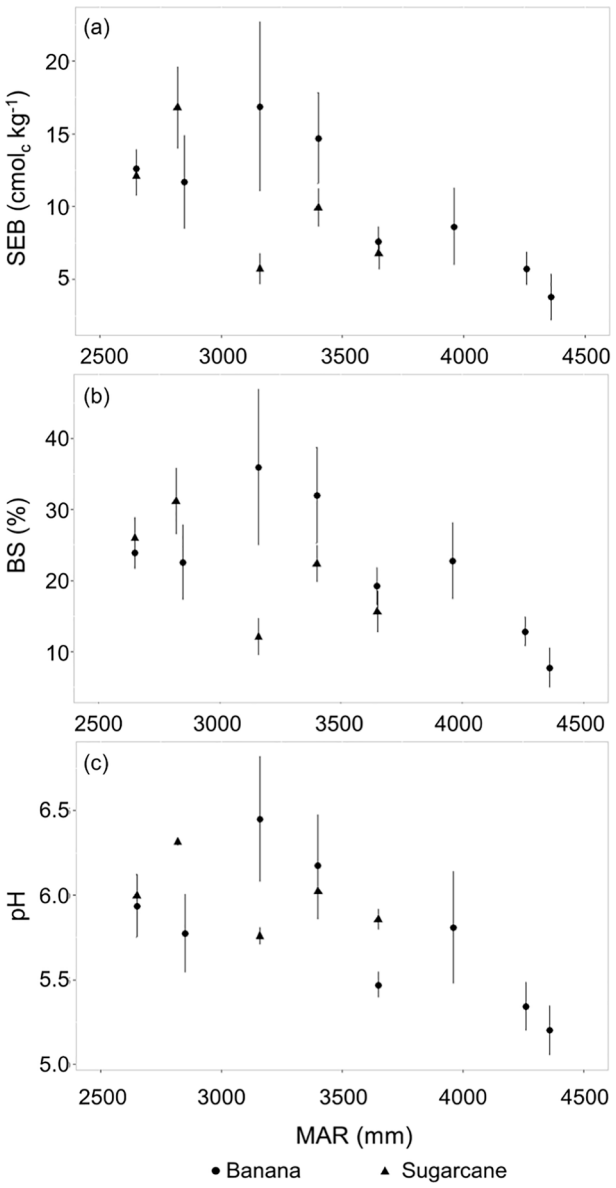

Fig. 7. Sum of exchangeable bases (SEB) (a), base saturation (BS) (b), and soil pH (c), as plotted against Mean Annual Rainfall (MAR). Error bars represent standard deviations.

(Fig. 8a–d, f). Rainfall was thus the main factor that affected the contents of total Si, plant available Si and phytolithic Si, as well as leaf Si, though to a much lesser extent. Actually, the range of leaf Si content (3.8–5.3 g kg^{-1}, Table 5) was higher than that measured by Henriet et al. (2008a) (1.8–3.9 g kg^{-1}) for bananas cropped on soils covering a similar range of TRB. Besides, leaf Si concentration in banana leaf may increase with the decrease of plant biomass with increasing MAR (Dorel et al., 2000), making Si mineralomass a better plant indicator of Si availability in soil. Rainfall directly controls the leaching intensity and the loss of elements (Chadwick et al., 2003), and was thus here the main parameter that controlled the availability of Si for plants. Since soil and climate conditions affect plant silicification patterns (de Tombeur et al., 2020) and plant tolerance to pathogens (Coskun et al., 2019), the impact of rainfall on Si bioavailability may explain the severe spread of fungal plant diseases previously reported in banana fields established on these perhydrated Andosols above 250 m asl (Dorel and Perrier, 1900; Kablan et al., 2012; Vermeire et al., 2011).

A surprising point is that rainfall has an opposite impact on the ox-Na_2CO_3-Si and XRD-*hl*PhSi pools (Fig. 8d, e). These pools are thus inversely correlated ($r = -0.88$, $p = 0.004$; Fig. 9). Both the ox-Na_2CO_3-Si and XRD-*hl*PhSi pools were associated to phytoliths through, respectively, chemical and physical extraction (Section 4.4). We propose that, in the studied soils, ox-Na_2CO_3-Si and XRD-*hl*PhSi contents do not represent the same phytolith pool.

5.6. *Quantification of different phytolith pools*

Phytoliths with different dissolution rates coexist in soil: fresh phytoliths quickly dissolve whereas aged ones dissolve slowly (Alexandre et al., 2011, 1997; Meunier et al., 2014). Strömberg et al. (2018) have distinguished labile from stable phytoliths, and suggested some preservation modes of fossil phytoliths. Li et al. (2020b) have proposed that the entrapment of phytoliths in soil aggregates may be one of the processes favoring the persistence of phytoliths in soils and sediments. We expect that this persistence should be enhanced in strongly aggregated soils such as the studied Andosols (Dorel et al. 2000). In fact, phytoliths in soil are considered as a major contributor to DSi because of their high dissolution rate (e.g., Alexandre et al., 2011; Bartoli, 1983; Farmer et al., 2005; Lucas et al., 1993; Sommer et al., 2013), while they are used as microfossils to reconstruct paleoenvironments due to their stability over millennia (e.g., Barboni et al., 1999; Cabanes et al., 2011; Kealhofer and Penny, 1998; Neumann et al., 2012; Rashid et al., 2019).

In this study, the ox-Na_2CO_3-Si and XRD-*hl*PhSi pools are inversely correlated to each other (Fig. 9). As assessed by Meunier et al. (2014), the chemical extraction using ox-Na_2CO_3-Si likely quantifies fresh phytoliths that dissolve quickly. In contrast, the physical extraction using heavy liquid separation (XRD-*hl*PhSi) would quantify the whole phytolith pool though it may dissolve some phytolithic particles during the alkaline DCB pretreatment.

In this line, we propose that, with increasing MAR, the pool of fresh phytoliths (ox-Na_2CO_3-Si) decreases while that of aged ones (XRD-*hl*PhSi) increases. The ratio [XRD-*hl*PhSi]/[ox-Na_2CO_3-Si] indeed increases from 0.33 to 11.0 with decreasing bulk density and increasing MAR (Fig. 10). As discussed here above (Section 5.5), rainfall directly controls the leaching intensity and the loss of elements (Chadwick et al., 2003). On one hand, rainfall and the rapid renewal of the soil solution increase the dissolution rate of fresh phytoliths. On the other hand, higher rainfall is associated with higher contents of secondary oxides and organic matter (Section 5.3), which positively influence soil aggregation in the studied soils (Dorel et al., 2000). Soil aggregates may entrap phytoliths and protect them from dissolution (Li et al., 2020b). Soil components such as SOM, OMA, ferrihydrite, Al hydroxide and allophanic substances all promote soil microaggregation (Bigham et al., 2002; Deng and Dixon, 2002; Harsh et al., 2002; Huang et al., 2002). The role of SRO Fe and Al oxides in soil microaggregation is further enhanced by their large surface area and reactivity (Bigham et al., 2002; Deng and Dixon, 2002; Huang et al., 2002). Since the contents of SOM, Al oxide, SRO Fe oxide increased with increasing MAR (Table 1), soil microaggregation probably increased with increasing MAR. This hypothesis is supported by the decrease in bulk density with increasing MAR (Table 1). The very strong inverse correlation between the ratio [XRD-*hl*PhSi]/[ox-Na_2CO_3-Si] and bulk density ($r = -0.97$) (Fig. 10) supports the hypothesis that the increasing dominance of aged phytoliths with increasing MAR could be linked to phytolith entrapment since bulk density is an indicator of soil aggregation. Thus, following Li et al. (2020b) and as supported by Fig. 10, we further hypothesize that soil microaggregation processes are intimately linked to phytolith stabilization processes. Within this view, phytoliths could be physically or chemically entrapped into microaggregates that protect them from dissolution. In the studied Andosols, the reactive phytolith surfaces (Bartoli, 1985; Fraysse et al., 2009) could possibly interact with SRO (Fe, Al) oxides, allophanic substances, SOM (Bartoli, 1985) in the overall process of soil microaggregation. These soil constituents may indeed promote the chemical or physical stabilization of phytoliths as their respective contents increase with increasing rainfall. This model may

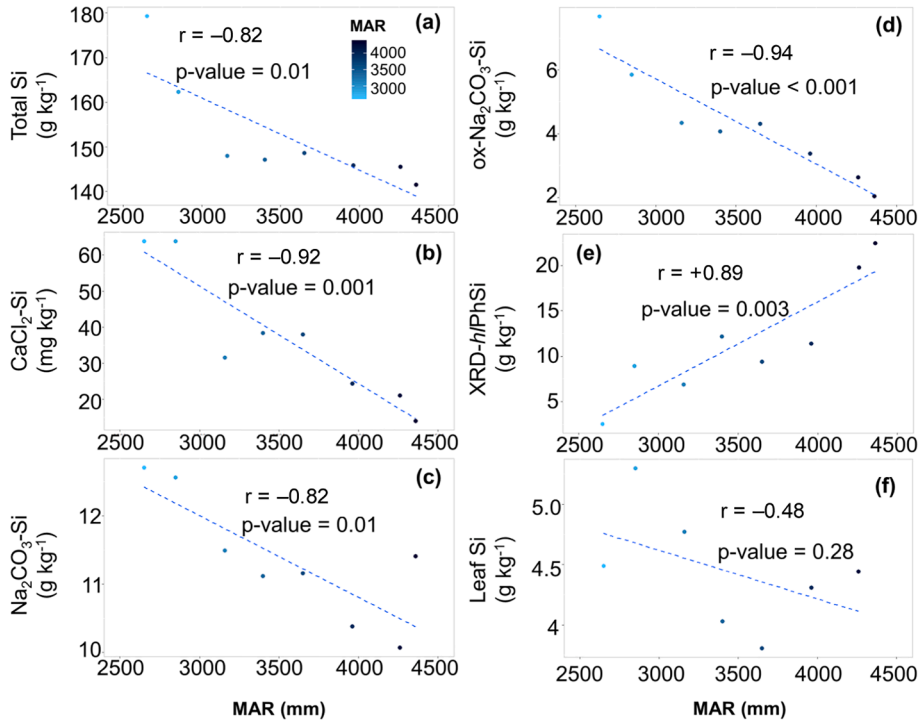

Fig. 8. Contents of total Si (a), $CaCl_2$-Si (b), Na_2CO_3-Si (c), ox-Na_2CO_3-Si (d), XRD-*hl*PhSi (e) concentrations in topsoil samples (banana and sugarcane plots); leaf Si concentration (banana, leaf III) (f), as plotted against MAR (Mean Annual Rainfall) with associated r and p values. The color of each point reveals the MAR level.

Table 5
Average concentrations in soil of total Si (Si_t), bioavailable Si ($CaCl_2$-Si), Na_2CO_3-Si, ox-Na_2CO_3-Si, and physically extracted PhSi, and Si concentration in banana leaf III. The average values are computed from individual values as determined on six composite samples collected in banana (3) and sugarcane (3) plots at 65, 100, 150, 200, and 250 m asl, but on three composite samples in banana plots at 300, 350, and 375 m asl, and at 396 m under forest. Different lowercase letters express significant differences at $p < 0.05$ level for Si_t, $CaCl_2$-Si, Na_2CO_3-Si, ox-Na_2CO_3-Si, banana leaf Si content. Differences were tested with a *t*-test with the pairwise.t.test function of the R programming language.

Altitude	Si_t	$CaCl_2$-Si	Na_2CO_3-Si	ox-Na_2CO_3-Si	XRD-*hl*PhSi[1]	Leaf Si (banana)
m	g kg^{-1}	mg kg^{-1}	g kg^{-1}	g kg^{-1}	g kg^{-1}	g kg^{-1}
65	179.3 a	65.5 a	11.2 a	7.68 a	2.54	4.49 ab
100	162.3 b	73.9 a	12.6 a	5.86 ab	8.94	5.30 a
150	148.0 c	31.3 bc	11.7 a	4.34 bc	6.90	4.77 ab
200	147.2 c	30.8 b	11.0 a	4.07 bc	12.16	4.03 b
250	148.6 c	31.1 b	11.5 a	4.30 bc	9.38	3.81 b
300	145.9 c	24.4 bc	10.4 a	3.37 bc	11.38	4.31 ab
350	145.6 c	21.1 bc	10.1 a	2.64 c	19.76	4.44 ab
375	141.5 c	14.0 c	11.4 a	2.04 c	22.45	nd[2]
396	128.7d	15.0 c	6.2 b	3.45 bc	nd	nd

[1] XRD-*hl*PhSi: phytolithic Si as assessed by XRD analysis after heavy liquid separation.
[2] nd refers to no data.

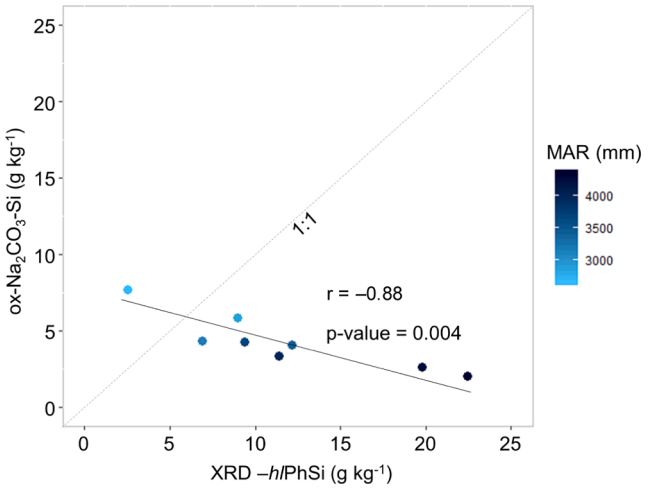

Fig. 9. Plot of the XRD-*hl*PhSi concentration against ox-Na_2CO_3-Si concentration in topsoil (0–20 cm) samples at each altitude (banana and sugarcane). The intensity of the blue color for each point reveals the MAR (Mean Annual Rainfall) level.

therefore explain the observed results.

5.7. Phytolith controls on plant available Si

Fig. 11 shows that $CaCl_2$–Si is positively and strongly correlated with ox-Na_2CO_3–Si ($r = +0.95$), but negatively correlated with XRD-*hl*PhSi ($r = -0.78$). The strong positive correlation between $CaCl_2$–Si and ox-Na_2CO_3–Si suggests that plant available Si was controlled by the pool of fresh phytoliths in soil that could quickly dissolve. The values of pH and H_4SiO_4 concentration in $CaCl_2$–Si extracts support that amorphous silica bodies controlled dissolved Si (Table S6). The controls exerted by phytoliths are governed by MAR since the lowest values of $CaCl_2$–Si and ox-Na_2CO_3–Si are both measured at the wettest sites (Fig. 11a).

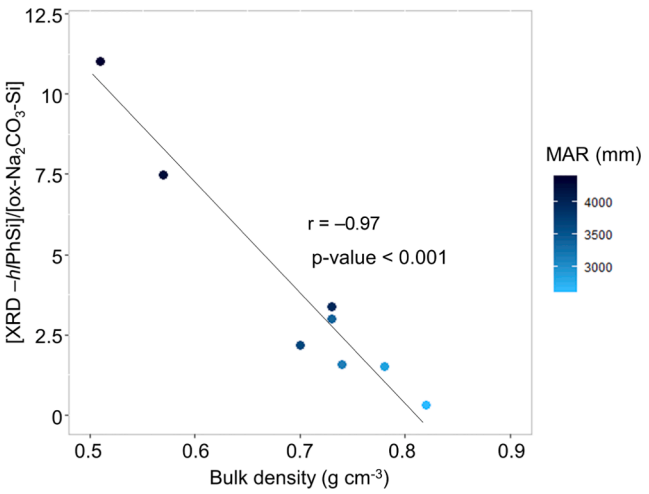

Fig. 10. Plot of the XRD-hlPhSi/ox-Na_2CO_3-Si ratio against the soil bulk density as measured in topsoils (0–20 cm) at each altitude. The bulk density is used as an indicator of the soil micro-aggregation process. The intensity of the blue color for each point reveals the MAR (Mean Annual Rainfall) level.

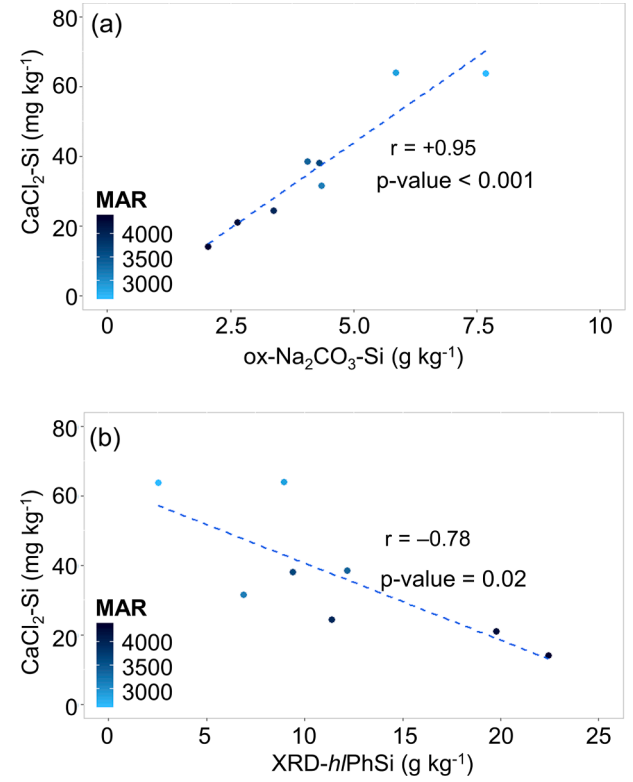

Fig. 11. Plot of $CaCl_2$-Si content against the contents of (a) ox-Na_2CO_3-Si and (b) XRD-*hl*PhSi in topsoil (0–20 cm) samples at each altitude. The intensity of the blue color for each point reveals the MAR (Mean Annual Rainfall) level.

Furthermore, our coupled experimental data ($CaCl_2$–Si, ox-Na_2CO_3–Si) are reasonably comparable with the literature data reported in Fig. 12 as well as to the range of coupled values [$CaCl_2$–Si, Na_2CO_3–Si] recently reported for humid tropical forests in Panama (see Fig. 1a in Schaller et al., 2018). In this latter study, within a MAR gradient from 1600 to 3200 mm, the ranges of $CaCl_2$–Si and Na_2CO_3–Si values were indeed 1–40 mg kg^{-1} and 1–7 g kg^{-1}, respectively (Schaller et al., 2018). Thus, as discussed above, the climatic controls on mineral synthesis in the studied Andosols led to advanced desilication and resulted in the formation of Fe oxide, aluminous allophane, gibbsite and poorly crystalline Al hydroxide. Furthermore, they resulted in the exhaustion of the buffering capacity with respect to ion exchange properties as previously reported (Chadwick et al., 2003), but also to plant available Si, likely because of the rapid dissolution of fresh phytoliths in strongly desilicated soil environments.

Aluminous character of ox-Na_2CO_3 extracts. In the ox-Na_2CO_3 extract, the [ox-Na_2CO_3–Si/ox-Na_2CO_3–Al] atomic ratio was ≤1.0, actually close to 1.0 in the less humid sites (Fig. 13a). Furthermore, the Si/Al atomic ratio of the ox-Na_2CO_3 extract sharply decreased from 1.0 to ~0.5 with increasing MAR below 3000 mm, but remained constant at ~0.48 at MAR > 3000 mm (Fig. 13b). Since the content of gibbsite increased while that of allophane decreased at MAR > 3000 mm, we attribute the ox-Na_2CO_3–Al content to (i) phytolith Al, and (ii) poorly crystalline Al hydroxide and possibly gibbsite (Huang et al., 2002). We can only speculate on how much poorly crystalline Al hydroxide occurred in the studied perhydrated Andosols because there are no unambiguous methods for its identification and quantification (Huang et al., 2002). We can argue that various environmental factors have promoted the formation of a series of Al-rich secondary products encompassing Al-humus, poorly crystalline Al hydroxide (Huang et al., 2002), gibbsite and aluminous allophane of proto-imogolite type (Churchman and Lowe, 2012; Harsh et al., 2002), added to Al-rich phytoliths. These environmental factors include (i) the rapid weathering of volcanic glass, (ii) the great intensity of leaching linked to high MAR and large porosity of ash material, (iii) the strong desilication, (iv) the accumulation of organic substances that can hamper the crystallization of gibbsite (Huang et al., 2002). On the other hand, the slow kinetics of macrocrystalline gibbsite formation enhance the precipitation of poorly crystalline and microcrystalline Al hydroxide at aqueous H_4SiO_4 of 10^{-4} mol l^{-1} where gibbsite should be stable (Harsh et al., 2002). When gibbsite is present as pseudomorphs of plagioclase and pyroxene, it will be present also in coarser fractions than <2 μm, as it occurs in neighboring perhydrated Andosols (Ndayiragije and Delvaux, 2003). This supports our hypothesis that there are two pathways for the formation of gibbsite in the studied Andosols: (i) direct formation of gibbsite *in situ* as pseudomorphs (Ndayiragije and Delvaux, 2003), and (ii) an indirect formation, not *in situ*, but through a stage of poorly crystalline, clay-sized Al hydroxide.

5.8. Critical assessment of the PhSi quantification methods

As illustrated in Fig. 9, our experimental data show significant differences in Si concentration between chemical extraction by alkaline dissolution (ox-Na_2CO_3-Si: 2–7.6 g kg^{-1}) and physical separation by heavy liquid (XRD-*hl*PhSi: 2.5–22.4 6 g kg^{-1}). As discussed above, the particular constitution of the studied soils may explain such discrepancies, which are particularly acute at the highest altitude levels.

The DeMaster technique using alkaline dissolution. The first point deals with the dissolution of phytoliths in Na_2CO_3 whereas the second one concerns the selectivity of Na_2CO_3 for phytoliths in an assemblage including phytoliths, SRO lithogenic silicate (LSi) and PSi minerals. *First*, Na_2CO_3 extractant mainly dissolves fresh phytoliths while it is less selective for aged phytoliths that poorly dissolve in Na_2CO_3 (Meunier et al., 2014). As discussed earlier (Section 5.6), we hypothesize that weathering, mostly governed by MAR, has promoted the ageing of phytoliths in soil, and probably their relatively high Al content (Fig. 13) (Bartoli, 1985) as well as their interactions with organic and mineral constituents in soil in the overall process of soil aggregation. *Second*, the Na_2CO_3 extraction dissolves SRO PSi minerals (Kamatani and Oku, 2000), and amorphous LSi components (Clymans et al., 2015). Besides, it dissolves wollastonite, a crystalline silicate (Li et al., 2019). Thus, the *DeMaster* technique (DeMaster, 1981) does not discriminate phytolith from SRO PSi and LSi minerals. Barão et al. (2014), Clymans et al. (2015), Kamatani and Oku (2000), and Koning et al. (2002) developed alternative techniques to discriminate PhSi from LSi and PSi SRO

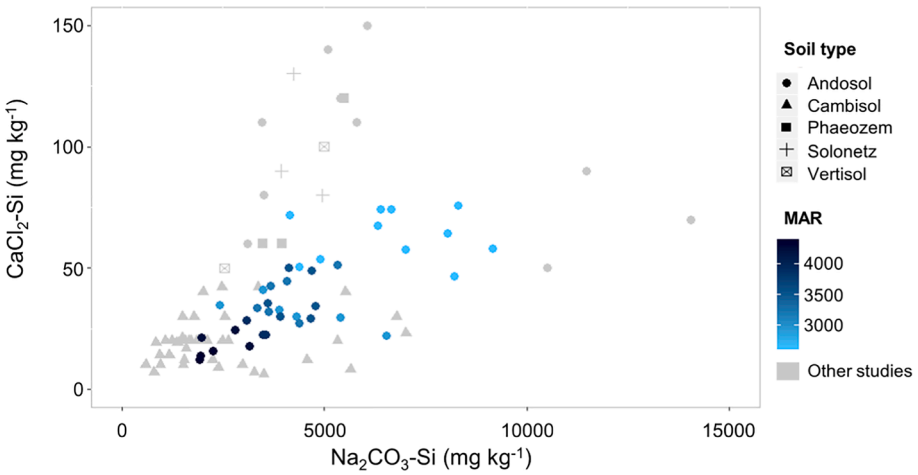

Fig. 12. Plot of $CaCl_2$-Si content against contents of Na_2CO_3-Si in different soil–plant systems. Light grey symbols are literature data for various soil types in temperate forests (Clymans et al., 2011; Cornelis et al., 2011), and tropical savannas (Quigley et al., 2017). Blue points are from this study and are ox-Na_2CO_3-Si values to discard the contribution of allophanic substances. The intensity of the blue color for each point reveals the MAR (Mean Annual Rainfall) level.

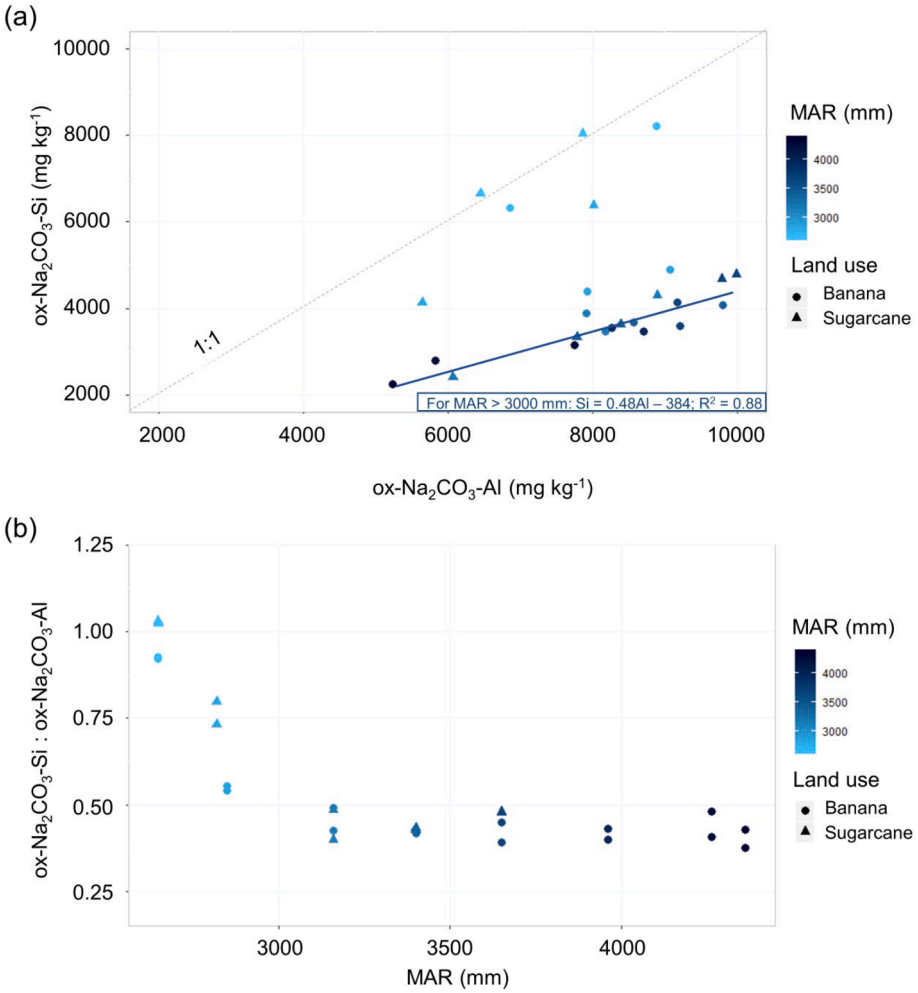

Fig. 13. (a) Plot of the ox-Na_2CO_3-Si concentration against ox-Na_2CO_3-Al concentration in topsoils (0–20 cm) at each altitude. Si and Al concentrations in the Na_2CO_3 extracts were derived using the technique of DeMaster (1981) on topsoil samples after allophane dissolution by dark oxalate (ox). (b) Plot of the evolution of the ox-Na_2CO_3–Si:Al ratio with increasing MAR (Mean Annual Rainfall). The intensity of the blue color for each point reveals the MAR level.

minerals based on the monitoring of the Si/Al atomic ratio during the kinetical alkaline extraction. Gibbsite, however, may dissolve in alkaline reagents (Huang et al., 2002), making the use of the Si/Al atomic ratio very hazardous, as shown in the present study. The procedure developed by Clymans et al. (2015) is also based on the use of the Si/Al atomic ratio to discriminate phytolithic Si from volcanic glass through a kinetical

alkaline extraction, but the presence of gibbsite makes this technique unusable. Here, the pretreatment of soil samples with dark oxalate buffered at pH 3 removed allophanic Si, i.e. Si from SRO PSi minerals. Given the advanced soil weathering stage in the studied Andosols, the pool of amorphous LSi minerals (volcanic glass) was considered as being exhausted. Much better than Na_2CO_3-Si, ox-Na_2CO_3-Si thus represented the PhSi pool since the dark oxalate pretreatment removed SRO PSi minerals with little effect, if any, on phytolith dissolution at pH 3 (Fraysse et al., 2009).

Heavy liquid separation. With regard to the extraction of phytoliths by heavy liquid separation, the presence of cristobalite, tridymite, and gibbsite prevents an accurate assessment of the phytolith content in the soil. Here, we propose a quantification of inorganic components occurring in the light fraction using SIROQUANT software. By doing so, we could evaluate the respective contents of phytolith, cristobalite, tridymite and gibbsite, and distinguish fresh from aged phytoliths.

6. Conclusion

The perhydrated Andosols under study have reached an advanced weathering stage. The climatic controls on mineral synthesis have resulted in the formation of Fe oxide, Al-rich allophane, gibbsite and poorly crystalline Al hydroxide. This mineralogical assemblage denotes intense leaching and strong desilication. In addition, the contents of SOM and (Al, Fe)-humus increased in the soils at the wettest sites. These climatic controls generate an abrupt threshold in soil properties at MAR $\geq$ 3000 mm. They have also led to (i) the exhaustion of the soil buffering capacity, (ii) the decrease in plant available Si and fresh phytolith content. Thus, within a narrow gradient of soil weathering degrees, the increase in MAR has resulted in the strong decrease in all Si pools in soil: pedogenic aluminosilicate, fresh phytolith and plant available Si. However, within the same gradient, an increasing amount of phytoliths was entrapped in soil aggregates, supporting the recognition of two phytolith pools. These pools involve fresh, labile phytoliths as an important source of bioavailable Si, and aged phytoliths preserved from dissolution within microaggregates.

We conclude that rainfall is the major, if not exclusive, driver of plant Si availability in the highly leached, gibbsitic Andosols from Basse-Terre, Guadeloupe.

We further conclude that research is required to improve the procedures quantifying phytolith content in soil and to investigate possible phytolith entrapment in soil microaggregates.

Declaration of Competing Interest

The authors declare that they have no known competing financial interests or personal relationships that could have appeared to influence the work reported in this paper.

Acknowledgments

C. Vander Linden is supported by the Belgian Science National Foundation for Scientific Research (FNRS), and the Research Foundation for Industry and Agriculture (FRIA) [F 3/5/5 – MCF/FC]. The research was supported by FNRS-FRIA N° 1.E061.16F and the 'Fonds Spécial de Recherche' of UCLouvain FSR-2016/FSR-2018. Z. Li is supported by FSR-2015, the Aspirant (ASP) – FNRS and Chargé de recherches (CR)-FNRS of Belgium. We warmly thank Alexis Durviaux for his constant involvement in field and laboratory work.

Appendix A. Supplementary data

Supplementary data to this article can be found online at https://doi.org/10.1016/j.geoderma.2021.115295.

References

Alexandre, A., Bouvet, M., Abbadie, L., 2011. The role of savannas in the terrestrial Si cycle: a case-study from Lamto, Ivory Coast. Glob. Planet. Change 78, 162–169.
Alexandre, A., Meunier, J.-D., Colin, F., Koud, J.-M., 1997. Plant impact on the biogeochemical cycle of silicon and related weathering processes. Geochim. Cosmochim. Acta 61, 677–682.
Anda, M., Dahlgren, R.A., 2020. Mineralogical and surface charge characteristics of Andosols experiencing long-term, land-use change in West Java, Indonesia. Soil Sci. Plant Nutr. 1–12.
Barão, L., Clymans, W., Vandevenne, F., Meire, P., Conley, D., Struyf, E., 2014. Pedogenic and biogenic alkaline-extracted silicon distributions along a temperate land-use gradient. Eur. J. Soil Sci. 65, 693–705.
Barboni, D., Bonnefille, R., Alexandre, A., Meunier, J.D., 1999. Phytoliths as paleoenvironmental indicators, West Side Middle Awash Valley, Ethiopia. Palaeogeogr. Palaeoclimatol. Palaeoecol. 152, 87–100. https://doi.org/10.1016/S0031-0182(99)00045-0.
Barrett, L.R., 2001. A strand plain soil development sequence in Northern Michigan, USA. Catena 44 (3), 163–186.
Bartoli, F., 1985. Crystallochemistry and surface properties of biogenic opal. J. Soil Sci. 36, 335–350.
Bartoli, F., 1983. The biogeochemical cycle of silicon in two temperate forest ecosystems. Ecol. Bull. 469–476.
Bartoli, F., Burtin, G., Herbillon, A.J., 1991. Disaggregation and clay dispersion of oxisols: Na resin, a recommended methodology. Geoderma 49, 301–317.
Beckwith, R.S., Reeve, R., 1963. Studies on soluble silica in soils. I. The sorption of silicic acid by soils and minerals. Soil Res. 1, 157–168.
Bigham, J.M., Fitzpatrick, R.W., Schulze, D.G., 2002. Iron oxides. Soil Mineral. Environ. Appl. 323–366.
Blakemore, L.C., 1983. Extractable iron, aluminium and silicon. Methods Chem. Anal. Soils 71–76.
Blakemore, L.C., 1981. Soil Bureau laboratory methods. A method for chemical analysis of soils. NZ Soil Bur. Sci. Pep. 10, A5–9.
Blecker, S.W., McCulley, R.L., Chadwick, O.A., Kelly, E.F., 2006. Biologic cycling of silica across a grassland bioclimosequence. Glob. Biogeochem. Cycles 20.
Brahy, V., Deckers, J., Delvaux, B., 2000. Incipient podzolization and weathering caused by complexation in a forest Cambisol on loess as revealed by a soil solution study. Eur. J. Soil Sci. 51 (3), 475–484.
Cabanes, D., Weiner, S., Shahack-Gross, R., 2011. Stability of phytoliths in the archaeological record: a dissolution study of modern and fossil phytoliths. J. Archaeol. Sci. 38, 2480–2490.
Cabidoche, Y.M., Feller, C., Larque, P., 1987. Sur un double mécanisme d'acidification des sols sous l'influence de cendres volcaniques récentes: le cas de la Soufrière de Guadeloupe après les éruptions de 1976–1977. C.R. Acad. Sci. Paris, 304, série II, 304(15), 935–939.
Chadwick, O.A., Gavenda, R.T., Kelly, E.F., Ziegler, K., Olson, C.G., Elliott, W.C., Hendricks, D.M., 2003. The impact of climate on the biogeochemical functioning of volcanic soils. Chem. Geol. 202, 195–223.
Chao, T., Sanzolone, R., 1992. Decomposition techniques. J. Geochem. Explor. 44, 65–106.
Charlier, J.-B., Lachassagne, P., Ladouche, B., Cattan, P., Moussa, R., Voltz, M., 2011. Structure and hydrogeological functioning of an insular tropical humid andesitic volcanic watershed: a multi-disciplinary experimental approach. J. Hydrol. 398, 155–170.
Churchman, G.J., Lowe, D.J., 2012. Alteration, Formation, and Occurrence of Minerals in Soils. CRC Press.
Clymans, W., Barão, L., Van der Putten, N., Wastegaard, S., Gísladóttir, G., Björck, S., Moine, B., Struyf, E., Conley, D.J., 2015. The contribution of tephra constituents during biogenic silica determination: implications for soil and palaeoecological studies. Biogeosciences 12, 3789–3804.
Colmet-Daage, F., Lagache, P., 1965. Caractéristiques de quelques groupes de sols dérivés de roches volcaniques aux Antilles françaises. Cah. L'ORSTOM Ser. Pédologie 8, 91–121.
Colmet-Daage, F., Lagache, F., 1969. Carte des sols des Antilles (Guadeloupe—Martinique). ORSTOM Antilles.
Cornelis, J.-T., Delvaux, B., 2016. Soil processes drive the biological silicon feedback loop. Funct. Ecol. 30, 1298–1310.
Cornell, R.M., Schwertmann, U., 2003. The Iron Oxides: Structure, Properties, Reactions, Occurrences and Uses. John Wiley & Sons.
Coskun, D., Deshmukh, R., Sonah, H., Menzies, J.G., Reynolds, O., Ma, J.F., Bélanger, R. R., 2019. The controversies of silicon's role in plant biology. New Phytologist 221 (1), 67–85.
Crabit, A., Cattan, P., Colin, F., Voltz, M., 2016. Soil and river contamination patterns of chlordecone in a tropical volcanic catchment in the French West Indies (Guadeloupe). Environ. Pollut. 212, 615–626.
Dagain, J., 1981. La mise en place du massif volcanique Madeleine-Soufrière, Basse-Terre de Guadeloupe, Antilles.
Dahlgren, R.A., 1994. Quantification of allophane and imogolite. Quant. Methods Soil Mineral. 430–451.
Dahlgren, R.A., Saigusa, M., 1994. Aluminum release rates from allophanic and nonallophanic andosols. J. Soil Sci. Plant Nutr. 40, 125–136. https://doi.org/10.1080/00380768.1994.10414285.
Delstanche, S., Opfergelt, S., Cardinal, D., Elsass, F., André, L., Delvaux, B., 2009. Silicon isotopic fractionation during adsorption of aqueous monosilicic acid onto iron oxide. Geochim. Cosmochim. Acta 73, 923–934.

Delvaux, B., Herbillon, A.J., Vielvoye, L., 1989. Characterization of a weathering sequence of soils derived from volcanic ash in Cameroon. Taxonomic, mineralogical and agronomic implications. Geoderma 45, 375–388.
DeMaster, D.J., 1981. The supply and accumulation of silica in the marine environment. Geochim. Cosmochim. Acta 45, 1715–1732. https://doi.org/10.1016/0016-7037(81)90006-5.
Deng, Y., Dixon, J.B., 2002. Soil organic matter and organic-mineral interactions. Soil Mineral. Environ. Appl. 69–107.
de Tombeur, F., Vander Linden, C., Cornélis, J.T., Godin, B., Compère, P., Delvaux, B., 2020. Soil and climate affect foliar silicification patterns and silica-cellulose balance in sugarcane (Saccharum officinarum). Plant and Soil 452 (1), 529–546.
Derry, L.A., Kurtz, A.C., Ziegler, K., Chadwick, O.A., 2005. Biological control of terrestrial silica cycling and export fluxes to watersheds. Nature 433, 728–731.
Dorel, M., Perrier, X., 1900. Influence du milieu et des techniques culturales sur la productivité des bananeraies de Guzadeloupe - Enquête diagnostic. Fruits 45 (3), 237–244.
Dorel, M., Roger-Estrade, J., Manichon, H., Delvaux, B., 2000. Porosity and soil water properties of Caribbean volcanic ash soils. Soil Use Manag. 16, 133–140.
Doumenge, F., 1985. Atlas des départements français d'Outre-Mer - 3 - la Guadeloupe, C. N.R.S.- O.R.S.T.O.M. Ann. Géographie 94, 492–493.
Drees, R., Wilding, L.P., Smeck, N.E., Senkayi, A.L., 1989. Silica in soils: quartz and disordered silica polymorphs. Miner. Soil Environ. 913–974.
Egli, M., Fitze, P., Mirabella, A., 2001. Weathering and evolution of soils formed on granitic, glacial deposits: results from chronosequences of Swiss alpine environments. Catena 45 (1), 19–47.
Eswaran, H., 1972. Micromorphological indicators of pedogenesis in some tropical soils derived from basalts from Nicaragua. Geoderma 7 (1–2), 15–31.
Farmer, V., Delbos, E., Miller, J., 2005. The role of phytolith formation and dissolution in controlling concentrations of silica in soil solutions and streams. Geoderma 127, 71–79.
Fieldes, M., Perrot, K.W., 1966. The nature of allophane in soils. I. Significance of randomness in pedogenesis. N. Z. J. Sci. 9, 622–632.
Fraysse, F., Pokrovsky, O.S., Schott, J., Meunier, J.-D., 2009. Surface chemistry and reactivity of plant phytoliths in aqueous solutions. Chem. Geol. 258, 197–206.
Fritsch, E., Balan, E., do Nascimento, N.R., Allard, T., Bardy, M., Bueno, G., Derenne, S., Melfi, A.J., Calas, G., et al., 2011. Deciphering the weathering processes using environmental mineralogy and geochemistry: towards a general model of laterite and podzol genesis in the Upper Amazon Basin. C. R. Geosci. 343, 188–198.
Garrels, R.M., Christ, C.L., 1965. Solutions, minerals and equilibria. Miner. Harper Row N. Y.
Godefroy, J., Dormoy, M., 1984. Un exemple d'utilisation du diagnostic sol à la programmation de la fertilisation en bananeraie. Fruits.
Harsh, J., Chorover, J., Nizeyimana, E., 2002. Allophane and Imogolite. Soil Mineral. Environ. Appl. sssabookseries, 291–322. https://doi.org/10.2136/sssabookser7.c9.
Haysom, M.B.C., Chapman, L.S., 1975. Some aspects of the calcium silicate trials at Mackay, in: Proceedings.
Heckman, K., Grandy, A.S., Gao, X., Keiluweit, M., Wickings, K., Carpenter, K., Carpenter, K., Horover, J., Rasmussen, C., 2013. Sorptive fractionation of organic matter and formation of organo-hydroxy-aluminum complexes during litter biodegradation in the presence of gibbsite. Geochim. Cosmochim. Acta 121, 667–683.
Henriet, C., Draye, X., Oppitz, I., Swennen, R., Delvaux, B., 2006. Effects, distribution and uptake of silicon in banana (*Musa* spp.) under controlled conditions. Plant and Soil 287, 359–374.
Henriet, C., Bodarwé, L., Dorel, M., Draye, X., Delvaux, B., 2008a. Leaf silicon content in banana (*Musa* spp.) reveals the weathering stage of volcanic ash soils in Guadeloupe. Plant Soil 313, 71–82.
Henriet, C., De Jaeger, N., Dorel, M., Opfergelt, S., Delvaux, B., 2008b. The reserve of weatherable primary silicates impacts the accumulation of biogenic silicon in volcanic ash soils. Biogeochemistry 90, 209–223.
Herbillon, A., 1986. Chemical estimation of weatherable minerals present in the diagnostic horizons of low activity clay soils, in: Proceedings of the 8th International Clay Classification Workshop: Classification, Characterization and Utilization of Oxisols (Part 1)[Beinroth, FH, Camargo, MN and Eswaran (Ed.)][39–48](Rio de Janeiro, 1986).
Herbillon, A.J., Frankart, R., Vielvoye, L., 1981. An occurrence of interstratified kaolinite-smectite minerals in a red-black soil toposequence. Clay Miner. 16, 195–201.
Huang, P.M., Wang, M.K., Kämpf, N., Schulze, D.G., 2002. Aluminum Hydroxides. Soil Mineral. Environ. Appl. sssabookseries 261–289. https://doi.org/10.2136/sssabookser7.c8.
IUSS Working Group WRB, 2014. World Reference Base for Soil Resources 2014. International soil classification system for naming soils and creating legends for soil maps. , World Soil Resources Reports 106. FAO, Rome.
Jien, S.H., Baillie, I., Huang, W.S., Chen, Y.Y., Chiu, C.Y., 2016. Incipient ferralization and weathering indices along a soil chronosequence in Taiwan. Eur. J. Soil Sci. 67 (5), 583–596.
Jones, L., Handreck, K., 1965. Studies of silica in the oat plant. Plant Soil 23, 79–96.
Jones, L.H.P., Handreck, K.A., 1963. Effects of iron and aluminium oxides on silica in solution in soils. Nature 198, 852–853. https://doi.org/10.1038/198852a0.
Jongmans, A.G., Buurman, P., van Doesburg, J.D.J., van Oort, F., Jaunet, A.M., 1994. Morphology, chemistry, and mineralogy of isotropic aluminosilicate coatings in a guadeloupe andisol. Soil Sci. Soc. Am. J. 58, 501. https://doi.org/10.2136/sssaj1994.03615995005800020036x.
Kablan, A.L., Lagauche, A., Delvaux, B., Legrève, A., 2012. Silicon reduces black sigatoka development in banana. Plant Dis. 96 (2), 273–278.
Kamatani, A., Oku, O., 2000. Measuring biogenic silica in marine sediments. Mar. Chem. 68, 219–229. https://doi.org/10.1016/S0304-4203(99)00079-1.
Katz, O., Lev-Yadun, S., Bar, P., 2013. Plasticity and variability in the patterns of phytolith formation in Asteraceae species along a large rainfall gradient in Israel. Flora 208 (7), 438–444.
Kealhofer, L., Penny, D., 1998. A combined pollen and phytolith record for fourteen thousand years of vegetation change in northeastern Thailand. Rev. Palaeobot. Palynol. 103, 83–93.
Keeping, M.G., Kvedaras, O.L., Bruton, A.G., 2009. Epidermal silicon in sugarcane: cultivar differences and role in resistance to sugarcane borer *Eldana saccharina*. Environ. Exp. Bot. 66 (1), 54–60.
Kelly, E.F., 1990. Methods for Extracting Opal Phytoliths from Soil and Plant Material: Workshop on Biotic Indicators of Global Change. Univ Wash.
Koning, E., Epping, E., Raaphorst, W.V., 2002. Determining biogenic silica in marine samples by tracking silicate and aluminium concentrations in alkaline leaching solutions. Aquat. Geochem. 8, 37–67. https://doi.org/10.1023/A:1020318610178.
Lacoeuilhe, J.-J., Godefroy, J., 1971. Un cas de carence en phosphore en bananeraie. Fruits 26, 659–662.
Leigh, D.S., 1996. Soil chronosequence of brasstown creek, Blue Ridge mountains, USA. Catena 26 (1–2), 99–114.
Li, Z., Unzué-Belmonte, D., Cornelis, J.-T., Vander Linden, C., Struyf, E., Ronsse, F., Delvaux, B., 2019. Effects of phytolithic rice-straw biochar, soil buffering capacity and pH on silicon bioavailability. Plant Soil 1–17.
Li, Z., Cornelis, J.T., Vander Linden, C., Van Ranst, E., Delvaux, B., 2020a. Neoformed aluminosilicate and phytogenic silica are competitive sinks in the silicon soil–plant cycle. Geoderma 368, 114308.
Li, Z., de Tombeur, F., Vander Linden, C., Cornelis, J.T., Delvaux, B., 2020b. Soil microaggregates store phytoliths in a sandy loam. Geoderma 360, 114037.
Lucas, Y., Luizao, F., Chauvel, A., Rouiller, J., Nahon, D., 1993. The relation between biological activity of the rain forest and mineral composition of soils. Science 260, 521–523.
Martin-Prével, P., 1980. nutrition minérale du bananier dans le monde-Première partie. Fruits 35, 503–518.
McKeague, J., Cline, M., 1963. Silica in soil solutions: II. The adsorption of monosilicic acid by soil and by other substances. Can. J. Soil Sci. 43, 83–96.
Mehta, S.K., Kalsotra, A., Murat, M., 1992. A new approach to phase transformations in gibbsite: the role of the crystallinity. Thermochimica acta 205, 191–203.
Meunier, J.-D., Colin, F., Alarcon, C., 1999. Biogenic silica storage in soils. Geology 27, 835–838.
Meunier, J.D., Keller, C., Guntzer, F., Riotte, J., Braun, J.J., Anupama, K., 2014. Assessment of the 1% Na2CO3 technique to quantify the phytolith pool. Geoderma 216, 30–35. https://doi.org/10.1016/j.geoderma.2013.10.014.
Monger, H.C., Kelly, E.F., 2002. Silica Minerals. Soil Mineral. Environ. Appl. sssabookseries, 611–636. https://doi.org/10.2136/sssabookser7.c20.
Ndayiragije, S., Delvaux, B., 2004. Selective sorption of potassium in a weathering sequence of volcanic ash soils from Guadeloupe, French West Indies. Catena 56, 185–198.
Ndayiragije, S., Delvaux, B., 2003. Coexistence of allophane, gibbsite, kaolinite and hydroxy-Al-interlayered 2: 1 clay minerals in a perudic Andosol. Geoderma 117, 203–214.
Nesbitt, H.W., Young, G.M., 1989. Formation and diagenesis of weathering profiles. J. Geol. 97, 129–147.
Neumann, K., Bostoen, K., Höhn, A., Kahlheber, S., Ngomanda, A., Tchiengué, B., 2012. First farmers in the Central African rainforest: a view from southern Cameroon. Quat. Int. 249, 53–62.
Nieuwenhuyse, A., van Breemen, N., 1997. Quantitative aspects of weathering and neoformation in selected Costa Rican volcanic soils. Soil Sci. Soc. Am. J. 61, 1450–1458.
Nizeyimana, E., Bicki, T.J., Agbu, P.A., 1997. An assessment of colloidal constituents and clay mineralogy of soils derived from volcanic materials along a toposequence in Rwanda. Soil Sci. 162, 361.
Norfleet, M.L., Karathanasis, A.D., Smith, B.R., 1993. Soil solution composition relative to mineral distribution in Blue Ridge Mountain soils. Soil Sci. Soc. Am. J. 57, 1375–1380.
Opfergelt, S., Georg, R.B., Delvaux, B., Cabidoche, Y.M., Burton, K.W., Halliday, A.N., 2012. Mechanisms of magnesium isotope fractionation in volcanic soil weathering sequences, Guadeloupe. Earth Planet. Sci. Lett. 341, 176–185.
Parfitt, R.L., Childs, C.W., 1988. Estimation of forms of Fe and Al - a review, and analysis of contrasting soils by dissolution and Mossbauer methods. Soil Res. 26, 121–144. https://doi.org/10.1071/sr9880121.
Parfitt, R.L., Russell, M., Orbell, G.E., 1983. Weathering sequence of soils from volcanic ash involving allophane and halloysite, New Zealand. Geoderma 29, 41–57. https://doi.org/10.1016/0016-7061(83)90029-0.
Parfitt, R.L., Wilson, A.D., 1985. Estimation of allophane and halloysite in three sequences of volcanic soils, New Zealand. Catena (Supplement 7), 1–8.
Parker, A., 1970. An index of weathering for silicate rocks. Geol. Mag. 107, 501–504.
Piperno, D.R., 1988. Phytolith Analysis: An Archaeological and Geological Perspective. Elsevier.
Quigley, K.M., Donati, G.L., Anderson, T.M., 2017. Variation in the soil 'silicon landscape' explains plant silica accumulation across environmental gradients in Serengeti. Plant Soil 410, 217–229. https://doi.org/10.1007/s11104-016-3000-4.
Rai, D., Kittrick, J.A., 1989. Mineral equilibria and the soil system. Miner. Soil Environ. 161–198.
Rashid, I., Mir, S.H., Zurro, D., Dar, R.A., Reshi, Z.A., 2019. Phytoliths as proxies of the past. Earth-Sci. Rev.
Raven, J.A., 1983. The transport and function of silicon in plants. Biol. Rev. 58, 179–207.

Rouiller, J., Burtin, G., Souchier, B., 1972. dispersion des sols dans l'analyse granulometrique, methode utilisant les resines echangeuses d'ions. Nancy Ecole Nat Super Agron Bull.

Sak, P.B., Navarre-Sitchler, A.K., Miller, C.E., Daniel, C.C., Gaillardet, J., Buss, H.L., Brantley, S.L., 2010. Controls on rind thickness on basaltic andesite clasts weathering in Guadeloupe. Chem. Geol. 276 (3–4), 129–143.

Samper, A., Quidelleur, X., Lahitte, P., Mollex, D., 2007. Timing of effusive volcanism and collapse events within an oceanic arc island: Basse-Terre, Guadeloupe archipelago (Lesser Antilles Arc). Earth Planet. Sci. Lett. 258 (1–2), 175–191.

Sangster, A., Hodson, M., 1986. Silica in higher plants. Silicon Biochem. 90–107.

Sauer, D., Saccone, L., Conley, D.J., Herrmann, L., Sommer, M., 2006. Review of methodologies for extracting plant-available and amorphous Si from soils and aquatic sediments. Biogeochemistry 80, 89–108.

Schaller, J., Turner, B.L., Weissflog, A., Pino, D., Bielnicka, A.W., Engelbrecht, B.M.J., 2018. Silicon in tropical forests: large variation across soils and leaves suggests ecological significance. Biogeochemistry 140, 161–174. https://doi.org/10.1007/s10533-018-0483-5.

Shoji, S., Dahlgren, R., Nanzyo, M., 1993. Chapter 1: terminology, concepts and geographic distribution of volcanic ash soils. In: Shoji, Sadao, Nanzyo, Masami, Dahlgren, Randy (Eds.), Developments in Soil Science, Volcanic Ash Soils. Elsevier, pp. 1–5. https://doi.org/10.1016/S0166-2481(08)70262-9.

Smithson, F., 1956. Plant opal in soil. Nature 178 (4524), 107.

Sommer, M., Jochheim, H., Höhn, A., Breuer, J., Zagorski, Z., Busse, J., Barkusky, D., Meier, K., Puppe, D., Wanner, M., Kaczorek, D., 2013. Si cycling in a forest biogeosystem – the importance of transient state biogenic Si pools. Biogeosciences 10, 4991–5007. https://doi.org/10.5194/bg-10-4991-2013.

Strömberg, C.A., Dunn, R.E., Crifò, C., Harris, E.B., 2018. Phytoliths in paleoecology: analytical considerations, current use, and future directions. In: Methods in Paleoecology. Springer, Cham, pp. 235–287.

van Breemen, N., Mulder, J., Driscoll, C., 1983. Acidification and alkalinization of soils. Plant Soil 75, 283–308.

Vander Linden C., 2019. Rainfall and land use control Si cycling in wet tropical Andosols. PhD thesis, UCLouvain, 262 p.

Vander Linden, C., Delvaux, B., 2019. The weathering stage of tropical soils affects the soil-plant cycle of silicon, but depending on land use. Geoderma 351, 209–220.

Vermeire, M.L., Kablan, A.L., Dorel, M., Delvaux, B., Risede, J.M., Legrève, A., 2011. Protective role of silicon in the banana-*Cylindrocladium spathiphylli* pathosysem. Eur. J. Plant Pathol. 31 (4), 621–630.

Wada, K., 1989. Minerals in Soil Environments. Soil Science Society of America.

Wada, K., 1977. Allophane and imogolite: in Minerals in the Soil Environments. In: Dixon, J.B., Weed, S.D., eds. Soil Sci. Soc. Am. Madison Wis.